Fundamental researches

UDC: 617.3:57.089.67:539.3 DOI: 10.26565/2313-6693-2022-44-01

QUANTUM, MOLECULAR AND CONTINUUM MODELING IN NONLINEAR MECHANICS OF VIRUSES

Zolochevsky O. O.[A,C,D,E,F]***, Parkhomenko S. S.***[B,C,D,E,F]***, Martynenko O. V.***[A,C,D,E,F]
(A – research concept and design; B – collection and/or assembly of data; C – data analysis and interpretation; D – writing the article; E – critical revision of the article; F – final approval of the article)

Introdution. Viruses are a large group of pathogens that have been identified to infect animals, plants, bacteria and even other viruses. The 2019 novel coronavirus SARS-CoV-2 remains a constant threat to the human population. Viruses are biological objects with nanometric dimensions (typically from a few tens to several hundreds of nanometers). They are considered as the biomolecular substances composed of genetic materials (RNA or DNA), protecting capsid proteins and sometimes also of envelopes.

Objective. The goal of the present review is to help predict the response and even destructuration of viruses taking into account the influence of different environmental factors, such as, mechanical loads, thermal changes, electromagnetic field, chemical changes and receptor binding on the host membrane. These environmental factors have significant impact on the virus.

Materials and methods. The study of viruses and virus-like structures has been analyzed using models and methods of nonlinear mechanics. In this regard, quantum, molecular and continuum descriptions in virus mechanics have been considered. Application of single molecule manipulation techniques, such as, atomic force microcopy, optical tweezers and magnetic tweezers has been discussed for a determination of the mechanical properties of viruses. Particular attention has been given to continuum damage–healing mechanics of viruses, proteins and virus-like structures. Also, constitutive modeling of viruses at large strains is presented. Nonlinear elasticity, plastic deformation, creep behavior, environmentally induced swelling (or shrinkage) and piezoelectric response of viruses were taken into account. Integrating a constitutive framework into ABAQUS, ANSYS and in-house developed software has been discussed.

Conclusion. Link between virus structure, environment, infectivity and virus mechanics may be useful to predict the response and destructuration of viruses taking into account the influence of different environmental factors. Computational analysis using such link may be helpful to give a clear understanding of how neutralizing antibodies and T cells interact with the 2019 novel coronavirus SARS-CoV-2.

KEY WORDS: *virus, mechanics, atomic force microcopy, stress, deformation, damage, healing, modeling, simulation*

INFORMATION ABOUT AUTHORS

Zolochevsky Alexander, D. Sc., Head of Laboratory, Research and Industrial Center «Polytech», 14, O. Yarosha st., Kharkiv, 61145; e-mail: zolochevsky55@ukr.net, ORCID ID: https://orcid.org/0000-0001-6632-4292

Parkhomenko Sophia, Researcher, Research and Industrial Center «Polytech», 14, O. Yarosha st., Kharkiv, 61145; e-mail: antiape41@gmail.com

Martynenko Alexander, D. Sc., Professor, Department of Hygiene and Social Medicine, V. N. Karazin Kharkiv National University, 6, Svobody sq., Kharkiv, Ukraine, 61022; e-mail: Alexander.v.martynenko@karazin.ua, ORCID ID: https://orcid.org/0000-0002-0609-2220

For citation:

Zolochevsky OO, Parkhomenko SS, Martynenko OV. QUANTUM, MOLECULAR AND CONTINUUM MODELING IN NONLINEAR MECHANICS OF VIRUSES. The Journal of V. N. Karazin Kharkiv National University. Series «Medicine». 2022: 44; P. 5–34. **DOI: 10.26565/2313-6693-2022-44-01**

INTRODUCTION

In the past reviews [1, 2, 3, 4], we focused the attention of readers on the nonlinear biomechanics of hard and soft tissues of living organisms. Due to the appearance of a number of important research questions [5] related to the recent outbreak of the 2019 novel coronavirus SARS-CoV-2 and fast spread of the disease COVID-19 around the world, we decided to present in this overview the applications of nonlinear mechanics to such biological structures as viruses. In this regard, the experimental, theoretical and computational studies of viruses and virus-like structures have been analyzed using models and methods of nonlinear mechanics.

According to Schrödinger [6], the biosphere is not an isolated thermodynamic system. Therefore, appearance and mutation of such disease-causing microorganisms as viruses are closely related to the evolution of cellular life. The general aim of the present review is to help predict the response and even destructuration of viruses taking into account the influence of different environmental factors. The environment is considered to be made up of those parts of the universal system with which the virus interacts [7]. Therefore, the influence of some environmental conditions like mechanical loads, thermal changes, electromagnetic field, chemical changes and receptor binding on the host membrane has been analyzed in the present review. These environmental factors have significant impact on the virus.

Viruses are a large group of pathogens that have been identified to infect humans, animals, plants, bacteria and even other viruses [8]. Viruses can be considered as the biomolecular substances composed of genetic materials (RNA or DNA), protecting capsid proteins and sometimes also of envelopes [9]. In other words, viruses consist of just a nucleic acid packaged within a protein shell and possibly also an envelope. Viral replication occurs by the inserting viral gene in host cells, and an envelope of the new formed virus particle derives from the host cell membrane. Building of the viral envelope involves proteins (glycoproteins), carbohydrates and lipids.

Different viruses range in structure, size, complexity and mechanisms of entry. RNA viruses are mostly single-stranded (ss) while DNA viruses may be either single-stranded or double-stranded (ds). The sizes of the entire infectious virus particles (virions) are in the range of a few tens to several hundreds of nanometers [9]. RNA viruses include the common cold, hepatitis C, hepatitis E, human immunodeficiency virus type 1 (HIV-1), West Nile, Ebola, influenza, norovirus (NV), mumps, rabies, Dengue, SARS-CoV (or SARS-CoV-1), MERS-CoV, SARS-CoV-2, polio and measles [10]. DNA viruses include adenoviruses, herpesviruses, in particular, herpes simplex virus type 1 (HSV-1), parvoviruses, papillomaviruses, polyomaviruses and poxviruses [10]. Genetic structure of viruses may be linear or circular. Capsids may consist of only one or a few structural protein species, and they may be formed as single- or multilayered protein shells [11]. Geometry of virus capsids follows helical (spiral) shape or icosahedral (quasi-spherical) symmetry. Viral envelope can be considered as additional protective shell in viruses. Schematic of virion structure of different viruses is given in Fig. 1a, b and c.

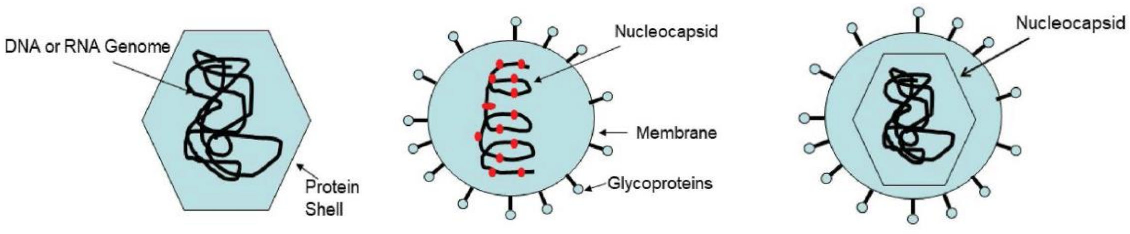

a b c

Fig. 1. Virion structure: Non-enveloped virus with icosahedral capsid structure (a), enveloped virus with helical nucleocapsid structure (b) and enveloped virus with icosahedral capsid structure (c) [10]

Three highly pathogenic variants of coronaviruses (enveloped, positive-sense single-stranded RNA viruses) have emerged in the 21st century, such as, severe acute respiratory syndrome-related coronavirus (SARS-CoV, 2002), Middle East respiratory syndrome-related coronavirus (MERS-CoV, 2012) and severe acute respiratory syndrome-related coronavirus-2 (SARS-CoV-2, 2019) [12]. Up to now, the novel coronavirus SARS-CoV-2, whose appearance was predicted 40 years ago in a fantastic novel [13], remains a constant threat to the human population. Schematic structure of the SARS-CoV-2 virion is presented in Fig. 2. It is seen (Fig. 2) that coronavirus particles comprise at least four structural protein species: spike (S), envelope (E), membrane (M) and nucleocapsid (N) [12]. The S protein including a large globular S1 domain and a rod-like S2 domain is responsible for receptor binding on the host cell surface.

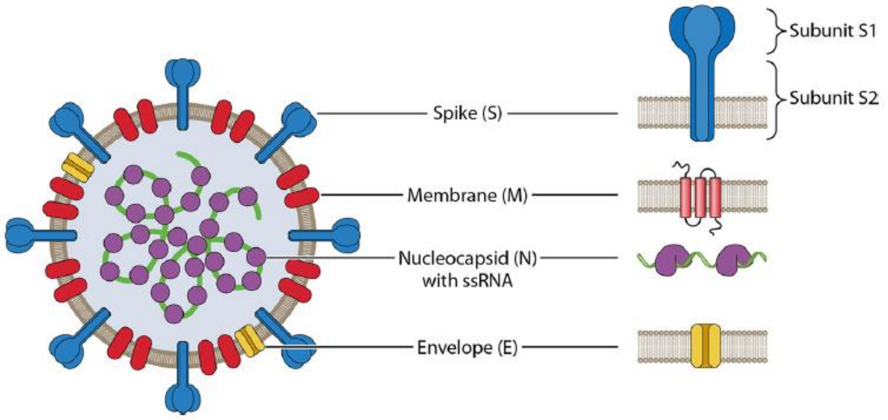

Fig. 2. Schematic SARS-CoV-2 structure and protein localization [12]

The atomic structure of viruses was studied in detail using X-ray crystallography and cryoelectron microscopy [14, 15]. After this it was established [16] that the most common simplifications for geometries of virions correspond to the sphere-like and rod-like particles, but spherocylinders, cones and other shell shapes are also available. For example, schematic of idealized capsid models is given in Fig. 3a, b for the spherical cowpea chlorotic mottle virus (CCMV) and the ellipsocylindrical bacteriophage $\phi 29$. Here, the average dimensions for the idealized models are accepted. It is clear (Fig. 3) that the capsid of $\phi 29$ virion can be considered as a thin shell [18, 19, 20, 21, 22] whiles the capsid of the CCMV virion as moderately thick shell [23, 24, 25].

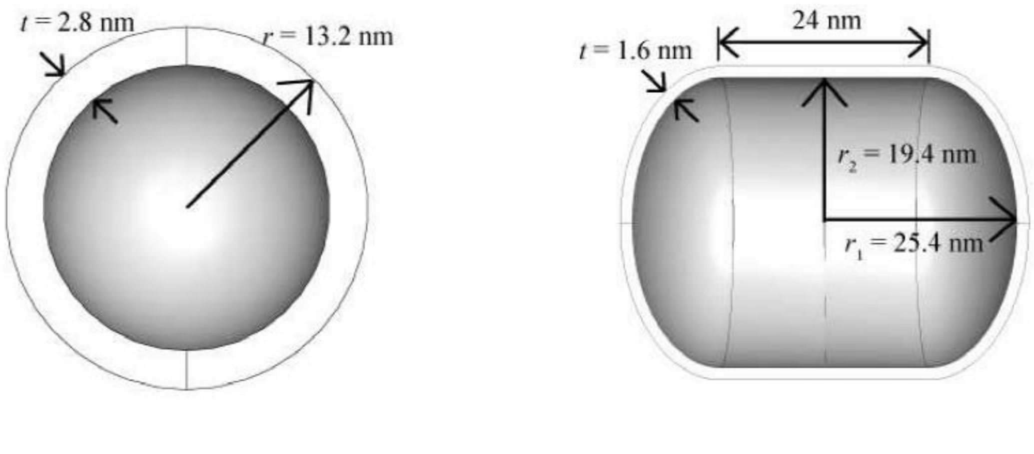

a **b**

Fig. 3. Schematic structure and model dimensions for the CCMV virion (a), and $\phi 29$ virion (b) [17]

Also, both tobacco mosaic virus (TMV) and M13 bacteriophage are rod-like particles of the cylindrical shape (Fig. 4a, b). M13 bacteriophage is 860 nm long and 6.5 nm in a diameter, while TMV is 300 nm long, 18 nm in a diameter [26]. Thus, the TMV and M13 virions can be considered as thick-walled cylinders [27–29].

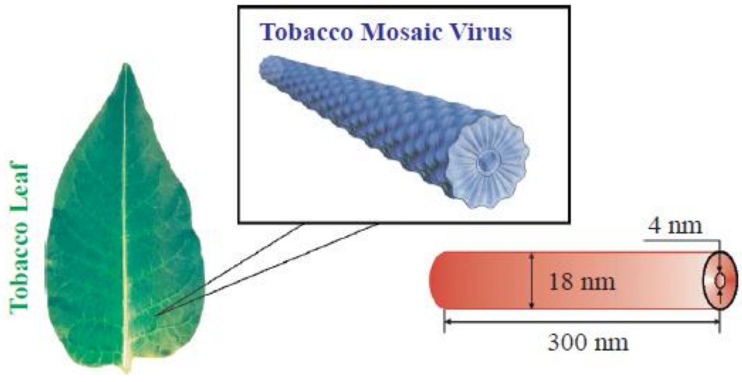

a

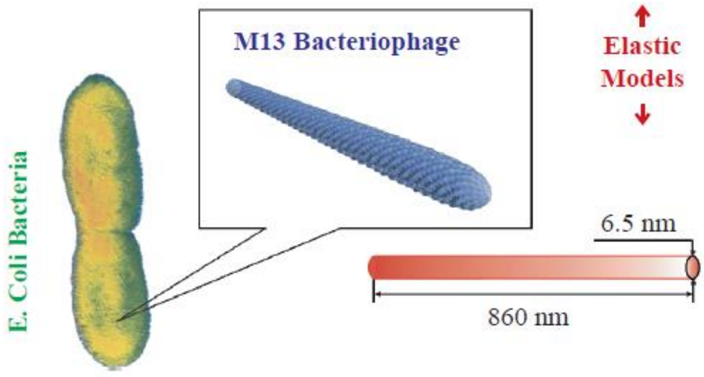

b

Fig. 4. Schematic structure and model dimensions for the TMV virion (a), and M13 virion (b) [26]

Additionally, the virion of a filamentous virus like Ebola can be considered approximately as a cylindrical particle. Furthermore, the Ebola virus has a diameter of about 80 nm, whereas its length can reach 1–2 μm [30]. Thus, filamentous viruses are cylindrical and long. On contrary, HIV, Zika and SARS-CoV-2 virions are nominally spherical virus particles. For example, a diameter of SARS-CoV-2 with spike (Fig. 2) is around 120 nm [30]. Note that virus shape affects the mechanical properties of viruses [31].

Virus infectivity is defined as the capacity of viruses to enter the host cell and exploit its resources to replicate and produce new infectious virions, which may lead to infection and subsequent viral disease in the human host [32, 33]. In order to initiate infection, viruses must enter host cells and deliver their genetic material. The most of viruses take the receptor mediated endocytic pathways (Fig. 5a, b) to enter host cells [34]. In this case, the plasma membrane binds specific macromolecules and smaller particles by means of cellular receptors, such as, sialic acids, integrins or cell adhesion molecules (Fig. 5a, b). Up to now, virus entry via endocytosis is not clear in detail. Depending on the virus, environment and cell type, viruses take a number of different endocytic pathways to gain entry. In general, there are several virus entry mechanisms with receptor binding on the host membrane. The first one (Fig. 5a) is related to clathrin and caveolin scaffolding in which the plasma membrane bending is assisted by clathrin/caveolin assembly [35]. The second one (Fig. 5b) is related to clathrin/caveolin-independent pathway in which membrane bending is driven by receptor-ligand binding [36]. A threshold virus particle radius, below which clathrin/caveolin independent endocytosis would not occur, was found to be about 12 nm for cylindrical and about 24 nm for spherical particles [37]. Thus, clathrin/caveolin-mediated endocytosis is the main virus' pathway from the extracellular space to the replication site [34].

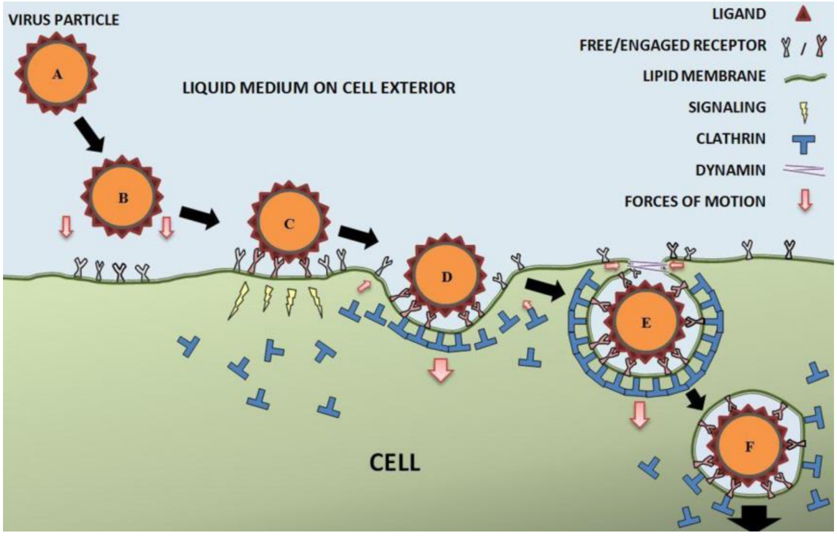

a

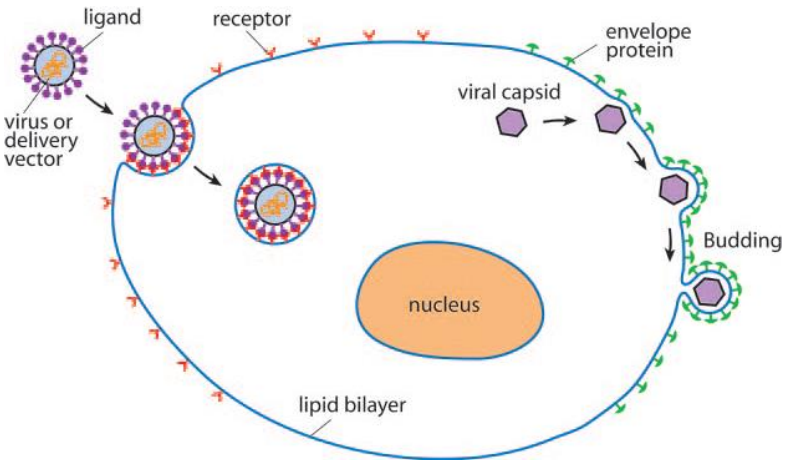

b

Fig. 5. Schematic illustration of the receptor-mediated endocytosis [34]: Stages of clathrin/caveolin-assisted pathway (a) [35], and clathrin/caveolin-independent pathway (b) [36]

After replication and production of new infectious virions, viruses must package their newly replicated genomes for delivery to other host cells. So, application of optical tweezers to pull on single DNA molecules of the bacteriophage $\phi 29$ virion, as they are packaged, shows that DNA-capsid complex under study is a force-generating motor [38]. The DNA is kept under high pressure (about 60 atm) inside the viral shell [38]. Furthermore, this large internal pressure may be available for initiating the ejection of the viral genome during infection. Thus, it is reasonable to expect the existence of external loads in virus entry mechanisms with receptor binding on the host membrane [34]. The initial events when a virus binds to cell surface receptors were quantified using an atomic force and confocal microscopy setup [39]. A generalized viral replication cycle [40] is given in Fig. 6. Understanding of virus entry via endocytosis and viral replication is very important for the development of antiviral strategies.

In 1997, Virus Mechanics was first introduced as a new research field by Falvo et al. [41] after determination of the Young's modulus (1.1 GPa) for the TMV (Fig. 4a). In this regard, atomic force microcopy (AFM) nanoindentation experiments, continuum approximation of rod-like virus and elastic bending theory of beams with circular cross section under point loading created by the AFM tip were used. It is interesting to note that the Young's modulus of virus is comparable with that of hard plastics. Also, the measured Young's modulus of virus is in the same order versus the values measured for structural proteins (about 4 GPa) [42], such as, collagen, actin or tubulin, and it is close to the values for bone (Fig. 7).

In the case of viral capsid proteins, there are strong covalent chemical bonds, and weaker noncovalent physical bonds that include electrostatic bonds (ion pairs and hydrogen bonds) and van der Waals bonds [42]. Therefore, deformation of viruses under mechanical loading arises from the stiffness of the bonds that hold the constituent atoms together.

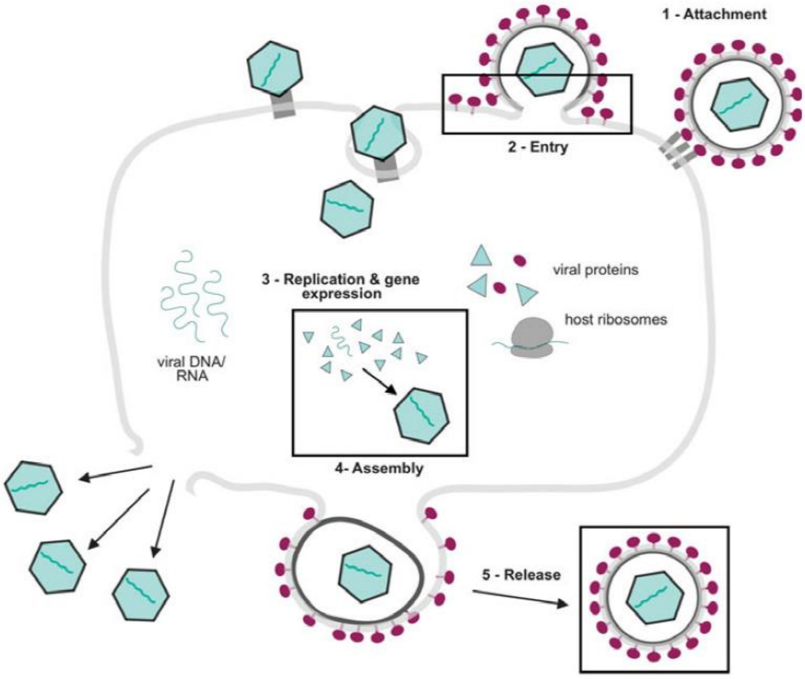

Fig. 6. Schematic viral replication cycle, showing the steps thought to be common to most viruses [40]

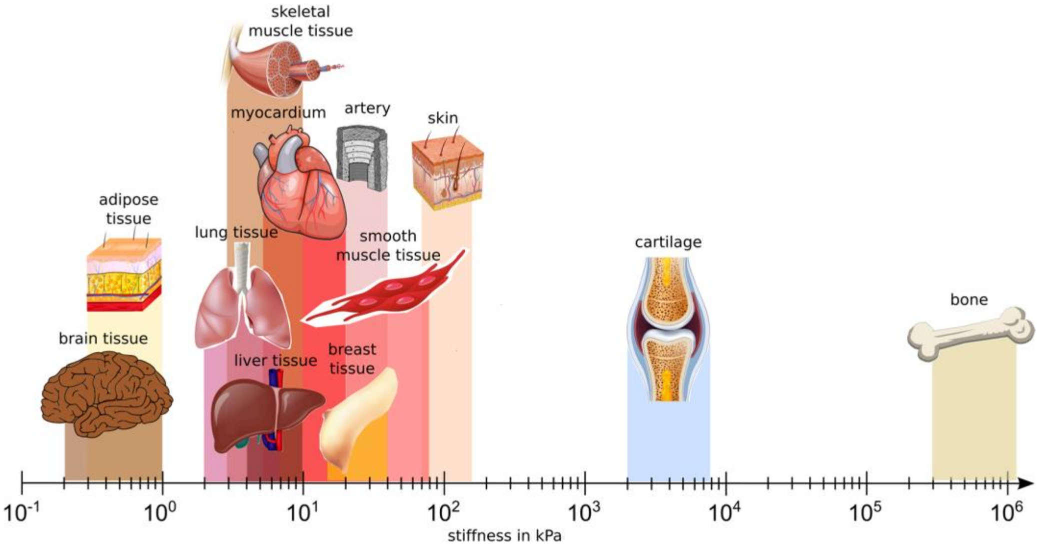

Fig. 7. Young's modulus of different tissues in the human body [43]

In general, a complete consideration of the mechanical response in nanosized objects would benefit from quantum, molecular and continuum descriptions [42, 44, 45].

Computational analysis methods in quantum modeling (first principles based modeling or ab initio calculations) of viruses are related to solving the many-particle Schrödinger equation directly. In this case, the interaction between particles (atoms) is dictated by their quantum mechanical state. Unfortunately, understanding of the atomic-scale interactions between the SARS-CoV-2 spike protein and the ACE2 receptor is limited by low amount of atoms taken in simulations [46], because ab initio calculations are highly computationally intensive even using supercomputer clusters. So, about 2 300 atoms were taken in the computational analysis given in [46]. At the same time, the cryoelectron microscopy structure of the SARS-CoV-2 spike (S) glycoprotein in the postfusion state has been well studied and widely reported [47]. In order to reduce computational costs, many fragment-like approaches to quantum modeling have been developed [48], in which fragments appear as groups of atoms, and the state of the full system is computed. An important advance of fragment-based methods is an approximate solution of the Schrödinger equation considering the separate blocks derived for individual fragments instead of the consideration of a quantum many-atom system.

The core of molecular modeling techniques (molecular dynamics or MD) relies on solving the second Newton's law to extract the positions of each atom and to obtain mechanical properties of viruses by employing the energy approach. In this way, deformation of virus has been considered in response to the ability to alter its conformation under the action of temperature fluctuations. The obvious advantage of MD simulations is the ability to access larger number of atoms, as well as, larger length scales and longer time scales using supercomputer clusters. So, the results of numerically simulated deformation by the AFM tip are presented for southern bean mosaic virus using the Lennard-Jones potential [49, 50]. The solvated viral capsid system with more than 4.5 million atoms was equilibrated for 13 ns and then force-indentation simulations were performed [49]. The effect of calcium removal on the mechanical properties of this RNA plant virus has been also studied [50]. Elastic properties of sesbania mosaic virus were determined from equilibrium thermal fluctuations of the capsid surface in molecular dynamics [51]. Simulation system with more than 800 000 atoms was equilibrated for 30 ns. Molecular simulations on the satellite tobacco necrosis virus (STNV) capsid were performed with 1.2 million atoms on the 1 μs time scale, exceeding any of the previous studies, and swelling of the viral capsid caused by calcium removal was predicted [52]. Molecular modeling technique was applied to generate equilibrium dynamics of the mature HIV-1 viral capsid [53]. Note that the HIV-1 retroviral capsid has a cone structure. Bending of the solvated viral capsid was numerically simulated for 100 ns at 2 fs time steps. Such capsid system with 64 million atoms is one of the largest biomolecular simulation systems in the world [54].

An alternative simulation technique in the MD is related to the consideration of virus as a system of coarse-grained particles instead of a system of atoms [55]. The simplification of a simulation system gives the possibility to reduce computational costs using coarse-grained models. In this way, several hundred atoms are represented by a single particle. Such level of coarse graining allows us to achieve the microsecond time scale. So, elastic deformation of the seven coarse-grained solvated viral capsid systems was simulated over time intervals of 1.5-25 μs [56]. In this regard, the four plant viruses (satellite tobacco mosaic virus STMV, satellite panicum mosaic virus, STNV and brome mosaic virus), poliovirus, bacteriophage ϕX174, and reovirus were studied. It is interesting to note that poliovirus and reovirus infect humans, whereas bacteriophage ϕX174 infects bacteria. Coarse-grained models on 35 different viral capsids were developed to simulate the AFM nanoindentation experiments [57]. The mechanical response of capsids and breaking of protein bonds were studied. Considering capsid deformation by the AFM tip, it was found that the force-indentation curve includes the elastic part and the irreversible one. The relationship between the mechanical properties of viruses and their structure has been discussed.

The other alternative approach in the MD studies of viruses is associated with lattice description considering viral capsid as a system of its structural units (capsomers) [58, 59]. In this way, combined AFM nanoindentation experiments and computational modeling on subsecond timescales of the CCMV capsid are considered. Unlike the double-stranded DNA bacteriophages, which can actively package their genetic material to internal pressures up to 60 atm [38], the filled plant CCMV capsid is not packed under pressure. It was taken into account in lattice description of virus that the capsid of CCMV is an icosahedral protein shell which is comprised of 60 trimer structural units with pentameric symmetry at the 12 vertices (pentamer capsomeres) and hexameric symmetry at the 20 faces (hexamer capsomeres) of the icosahedron [58, 59]. Simulations were carried out in the isolated single pentamer and hexamer capsomers, as well as, in the full CCMV capsid at equilibrium. Computational studies show two dynamic regimes to be responsible for the CCMV capsid stiffening and softening. In particular, stiffening at low force (or indentation) is similar to Hertz response for solid bodies in contact. The large-amplitude out-of-plane displacements mediate the capsid bending which is in direct contact with collapse of the biological structure. It was numerically established that reversibility and irreversibility of indentation are correlated with the mechanical characteristics, i.e., elastic deformation and inelastic response due to local rearrangements of the capsid proteins. Such investigations can help to understand on how the CCMV can infect plant tissue through damaged cell walls that can be produced by either mechanical or biological means. For example, swelling of virus may be related to its mechanism of infectivity.

Continuum description of viruses is constructed using well developed models and methods of solid mechanics [27, 60, 61]. In 2004, Ivanovska et al. [62] determined the Young’s modulus (around 1.8 GPa) for the bacteriophage $\phi29$ based on the AFM nanoindentation experiments, Hertz model and theory of elastic thin spherical shells. It is interesting to note that the Young’s modulus of $\phi29$ is larger than that of the TMV [41]. Unlike [41], paper by Ivanovska et al. [62] was a start for the numerous studies of linear elastic deformation for such viruses of the spherical shape as CCMV, bacteriophages λ and HK97, murine leukemia virus (MLV), minute virus of mice (MVM), STMV, Wiseana iridovirus (WIV), and hepatitis B virus (HBV) [63–71]. Nonlinear finite element analysis of spherical viruses using AFM nanoindentation was given in [17, 63, 64, 66, 69, 70, 72–76]. The mechanical response of viruses has been found to depend on the packed genome. The linear elastic bending theory of beams with circular cross section was applied to the rod-like TMV virion [77] by analogy with Falvo et al. [41]. Nonlinear finite element modeling of the TMV capsid at the AFM nanoindentation has been considered in [78]. The radial Young’s modulus of the TMV [78, 79] determined using the Hertz model is comparable with the axial Young’s modulus [41]. Thus, it is possible to assume the initial isotropy of the TMV. In general, continuum techniques are the preferable methods to simulate the mechanical behavior of viruses. At the same time, replacing a discrete structure of virus with a continuum media is the most critical part of modeling process.

Both MD and continuum modeling are employed for mechanical characterization of virus capsids taking into account prestresses and linear elasticity [80]. Also, molecular and continuum levels of description were applied to the nonlinear analysis of HK97, CCMV and HBV at the AFM nanoindentation [71, 81]. Multiscale simulations in Virus Mechanics are actually rare.

Regarding the simulation of the viral entry into a cell membrane via endocytosis (Fig. 5), such important aspects were involved as the contact mechanics of viruses onto a flexible membrane [30, 82, 83 ,84, 85], effects of virus size and ligand density on the membrane wrapping [86], as well as, influence of receptor concentration gradient on the ligand-receptor binding [87]. The change of receptor density over the host membrane was described [37, 88, 89] by the Fick's second law [90, 91, 92], however, without consideration of diffusion induced stresses [93, 94, 95, 96, 97, 98]. Continuum modeling was used for adhesive contact between the virus and cell membrane, driven by adhesion [82, 83, 84] or driven by adhesion and, additionally, by external displacement (or force) [30, 85], however, under the assumption of linear elasticity. Thus, a little is known about the nonlinear biomechanical interactions between ligand and receptor molecules. Therefore, up to now, antiviral strategy based on the nonlinear mechanics of viruses has not yet been developed.

MATERIALS AND METHODS

Mechanically, virus behaves identically to any other elastoviscoplastic material in that it undergoes large deformation when subject to different environmental factors (mechanical load, light, magnetic field). In this regard, application of single molecule manipulation techniques, such as, AFM, optical tweezers and magnetic tweezers has been given for a determination of the mechanical properties of viruses [99].

AFM nanoindentation. Since its invention in 1986, the AFM has been the most widely used scanning probe microscope for biological applications [100]. Unfortunately, a tutorial for laboratory training of Ukrainian students and young specialists in virology does not include the use of the AFM [101]. The majority of AFM experiments on viruses are performed by nanoindentation (Fig. 8a, b, c) [102, 103, 104].

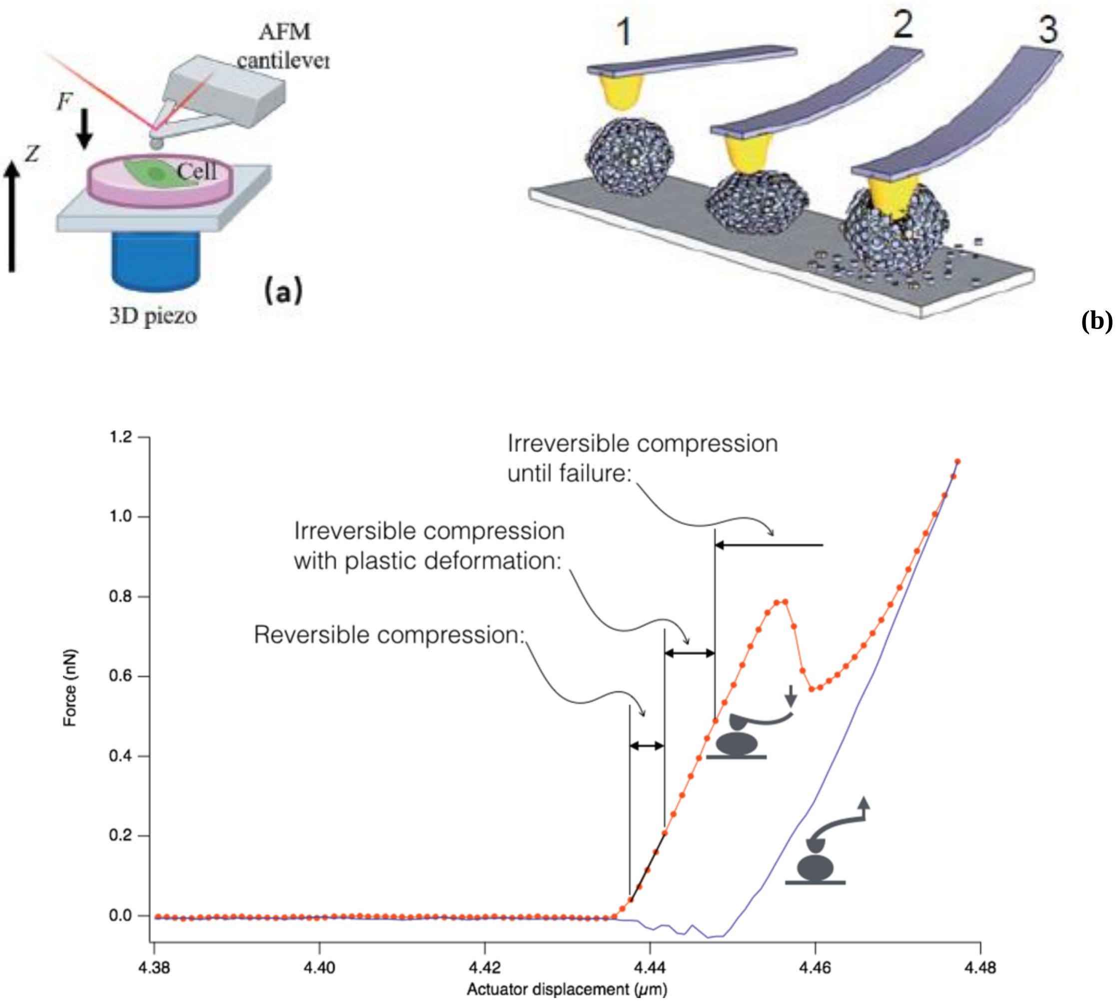

(c)

Fig. 8. AFM nanoindentation: Schematics (a), three main phases of experiments (b): before contact (1), during indentation (2) and after breaking (3), and force–piezoactuator displacement curve for single brome mosaic virus [102-104]

The AFM uses sharp spherical (or conical) tip (often with radius of curvature about or below 10 nm) mounted at the free end of a cantilever. The characteristic feature of AFM nanoindentation test with probes attached to the end of cantilever beams is related to the principal opportunity for detection of attractive/repulsive forces between the probing tip and the sample surface in excess of 10 pN [99]. Taking into account that the indenter contacts the surface of the sample, the displacement of the cantilever base is translated into the indentation depth and the deflection of cantilever [104]. The indentation force F (Fig. 8a) can be determined by the deflection of the cantilever, and the indentation depth δ can be calculated from the position of the 3D piezoelectric actuator. It is clear (Fig. 8c) that the force-displacement curve at loading reflects both elastic and plastic properties of virus. Also, the failure of virus occurs at indentations between 20 % and 30 % of the virus diameter and between 0.6 nN and 1.2 nN of the applied force [104]. Limitations of this technique are large high-stiffness probe and large minimal force [99].

Optical tweezers. Optical trapping (or optical tweezers) can manipulate individual virus particles using low-power near-infrared laser beams. In this way, light scattering imaging (Fig. 9 a, b) is the most often used method based on the measurement of the change in a signal or light scattering by individual virus particles at a given angle with time [105, 106]. The scattered light contains both elastic and inelastic components. Optical tweezers with the three dimensional manipulation and small low-stiffness probe have been developed to exert forces in excess of 0.1 pN [99]. Limitations of such technique are sample heating and photodamage. In one of the first applications of optical tweezers in Virus Mechanics [68], the Young's modulus of the wet STMV crystal was found to be 3.3 GPa. This value is comparable with that of the bacteriophage $\phi 29$ (around 1.8 GPa) by Ivanovska et al. [62].

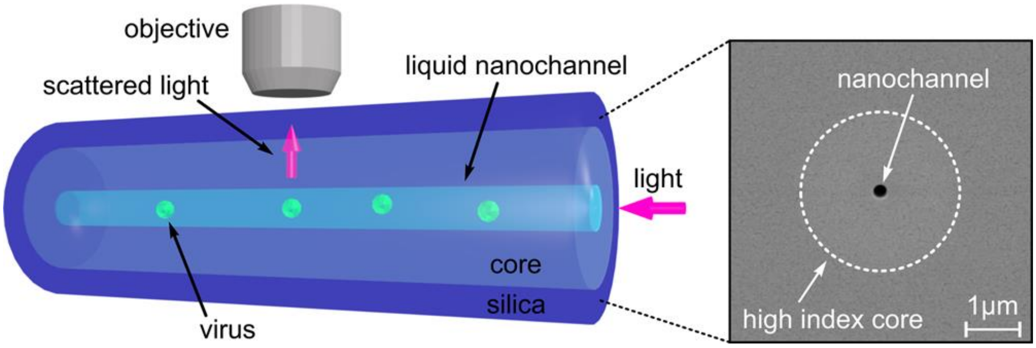

a

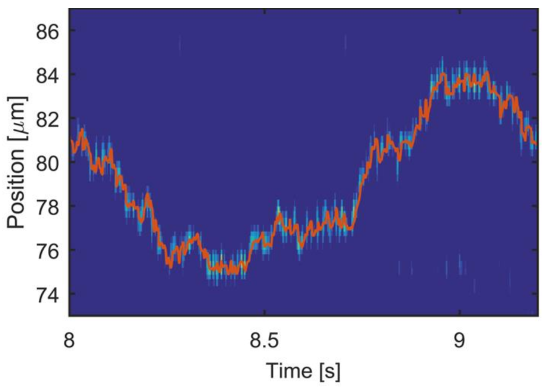

b

Fig. 9. Light scattering of single virus particles in a nanofluidic optical fiber: Schematic of the apparatus and an SEM image of the fiber cross section (a), and detected position of a freely diffusing CCMV particle in water with time [105]

Magnetic tweezers. Magnetic manipulation is extremely selective for the magnetic beads used as probes,

and the single molecules under study are tethered between a flow cell surface and magnetic beads. Magnetic tweezers (MT, Fig. 10a, b) and electromagnetic tweezers (MT designed with electromagnets, Fig. 10c) are the most straightforward of the three single molecule manipulation techniques to implement [99, 107]. Furthermore, novel kinds of this technique (Fig. 10 b, c) allow us to directly observe torque and twist of nucleoprotein complexes and viral genomes. Magnetic (electromagnetic) tweezers have been developed to exert forces in excess of 10^{-3}(0.01) pN [99]. Also, the spatial and temporal resolutions of such technique are higher than optical tweezers and AFM.

Conventional MT (Fig. 10a) consist of two cubic permanent magnets that produce a horizontal magnetic field and induce the stretching of molecules in X, Y and Z directions [107]. As an example, Fig. 11 shows the experimental data for force-extension in Z direction of double-stranded RNA molecule [108].

The use of cylindrical magnets and additional side magnet in MT (Fig. 10b) gives the possibility to apply the magnetic torque. The advantage of electromagnets (Fig. 10c) is that force and rotation can be controlled by changing the current rather than moving the magnets. However, unlike optical tweezers, electromagnetic tweezers do not create a stable three-dimensional trapping potential [107]. Limitation of electromagnetic tweezers is hysteresis in the magnetic field as a function of current.

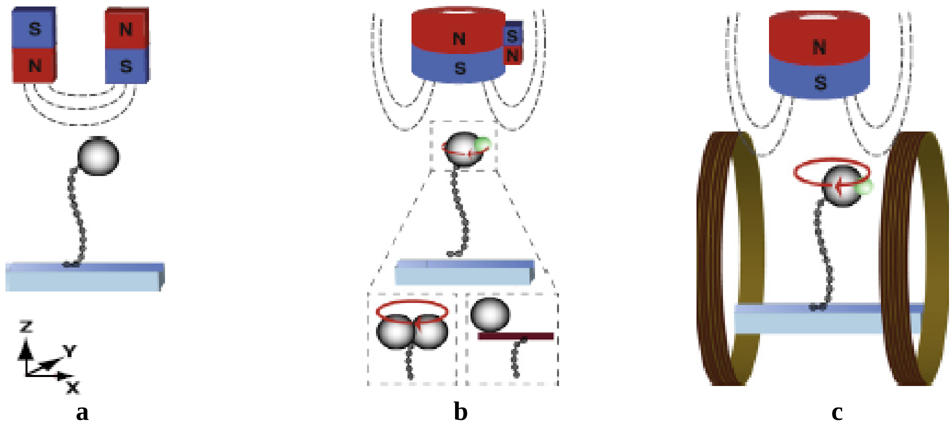

Fig. 10. Schematics of magnetic and electromagnetic tweezers: Conventional MT (a), magnetic torque tweezers with cylindrical magnets and additional side magnet (b), electromagnetic torque tweezers with Helmholtz coils around cylindrical magnets (c) [107]

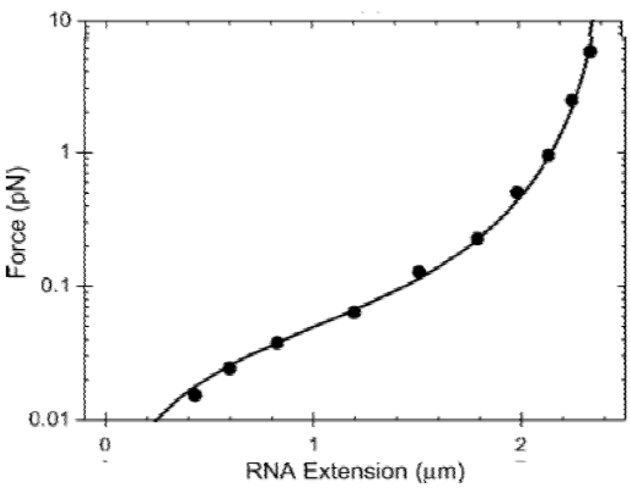

Fig. 11. Force-extension measurements using conventional MT for dsRNA [108]

Mechanical properties of viruses. Experimental data obtained by means of AFM, optical tweezers and magnetic tweezers can be used for nanomechanical characterization of the deformation response of viruses affected by different environmental factors (mechanical loads, chemical changes, thermal changes, electromagnetic field and receptor binding on the host membrane).

In particular, a reversible linear elastic regime was observed for AFM nanoindentation of virus capsids when the indentation did not exceed 20–30 % of the capsid thickness [109]. As known [102], in the case of spherical capsids and spherical probes, the relation between the indentation force *F* and the indentation depth δ can be described mathematically by different contact models of continuum mechanics given in Table 1. Here, *E* is the Young's modulus of a virus; ν is the Poisson's ratio of a virus; *R* is the probe radius; *a* is the contact area radius; *h* is the thickness of viral capsid; F_{AD} is the adhesion force; χ_S is the correction parameter, $\chi_S = \sqrt{R\delta / h}$. Most of the studies of linear elastic deformation during AFM nanoindentation refer to the application of the Hertz analysis [110]. However, the Hertz formulation of the contact problem (Table 1) leads to incompatibility of displacement fields due to the, first, geometrically linear formulation and, second, due to the ignoring the appearance of the tangential displacements [111, 112]. In other words, the Hertz analysis was done for frictionless and nonslipping boundary conditions under assumption that $\delta << R$. In contrary, the Sneddon model (Table 1) was developed for large indentation [113]. The Derjaguin–Müller–Toporov (DMT) [114] and Johnson–Kendall– Roberts (JKR) [115] formulations in Table 1 can be used in cases of small and large adhesion, respectively. The finite thickness correction (FTC) was used by Dimitriadis et al. [116] to introduce an approximation dependent on probe radius, thickness and indentation, as polynomial expansion of the correction parameter χ_S, considering sample bound to substrate (FTC bound in Table 1) or free to move (FTC free in Table 1).

Table 1

Interpretation of AFM nanoindentation measurements for spherical tip and spherical virus [102]

Model	Equation(s)	
Hertz	$F = \frac{4}{3}\frac{E\sqrt{R}}{(1-\nu^2)}\delta^{3/2}$	
Sneddon	$F = \frac{E}{2(1-\nu^2)}\left[(a^2+R^2)\ln\left(\frac{R+a}{R-a}\right) - 2aR\right]$	$\delta = \frac{1}{2}a\ln\left(\frac{R+a}{R-a}\right)$
DMT	$F = \frac{4}{3}\frac{E\sqrt{R}}{(1-\nu^2)}\delta^{3/2} + F_{AD}$	
JKR	$F = \frac{4Ea^3}{3R(1-\nu^2)} - \sqrt{\frac{16EF_{AD}}{3(1-\nu^2)}a^3}$	$\delta = \frac{a^2}{R} - \sqrt{\frac{4F_{AD}(1-\nu^2)}{ER}a}$
FTC bound	$F = \frac{4}{3}\frac{E\sqrt{R}}{(1-\nu^2)}\delta^{3/2}[1 + 1.133\chi_S + 1.283\chi_S{}^2 + 0.769\chi_S{}^3 + 0.0975\chi_S{}^4]$	
FTC free	$F = \frac{4}{3}\frac{E\sqrt{R}}{(1-\nu^2)}\delta^{3/2}[1 + 0.884\chi_S + 0.781\chi_S{}^2 + 0.386\chi_S{}^3 + 0.0048\chi_S{}^4]$	

Thus, the Young's modulus of a virus can be derived from the slope of the force-indentation curves taking into account that the indenter size, the Poisson's ratio of a virus and the thickness of the viral capsid are known. Note also that the Poisson's ratio of viruses can take a range of values from 0.3 to 0.5 [17, 62, 117–124]. Unfortunately, the Hertz model is affected by harsh limitation to be carefully considered upon application on viruses: indentation must be small compared with probe radius [102], i. e., it should be $\delta << R$. To get around this limitation, the solution of the theory of thin spherical shells by Reissner [125] was used [126], such as

$$F = \frac{4Eh^2}{\sqrt{3}r\sqrt{1-\nu^2}}\delta, \qquad (1)$$

where *r* is the radius of the middle surface of viral capsid. Also, in the case of conical AFM tip and spherical virus the Hertz formulation [110] can be presented as follows [127]

$$F = \frac{2}{\pi}\frac{E\tan\alpha}{1-\nu^2}\delta^2, \qquad (2)$$

where α is the semivertical angle of a cone.

Table 2 summarizes the available information about the Young's moduli of viruses. It is an extension of the experimental data given in reviews [16, 109, 128].

Capturing the elastic effects of the presence of nucleic acids polymers (DNA and RNA) in viruses is a way to gain insight into the physicochemical aspects of virus infectivity [129]. Note that deformation by compressing, stretching and twisting is vital for genome packaging. Compression elements of genome resist pushing, while tension elements resist pulling.

Table 3 provides all the necessary information about the Young's moduli of genomes [130, 131,132, 133, 134, 135, 136, 137, 138, 139, 140]. The freely jointed chain model and the worm-like chain model developed in the theory of entropic elasticity of genomes could not be applied to reproduce such data using different methods of measurement [141]. Therefore, the concepts of solid mechanics [27, 60, 61] were used with continuum description of genomes. In this way, the single molecule of DNA is considered as a straight rod of the circular cross section (initial radius r_0 and initial length l_0) under axial loading. Additionally, the average dimensions of DNA are accepted, such as, $r_0 = 1$ nm, as well as, $l_0 = 50$ nm (long molecules [130, 131,132, 133, 134, 135, 136, 139, 140]), and $l_0 = 10$ nm (short molecules [137, 138]) in the idealized elastic model [130, 131, 135, 137, 140]:

$$F = \frac{\pi r_0^2 E}{l_0}\delta \qquad (3)$$

Also, the Hertz-type contact models are used for the AFM nanoindentation [134, 136, 138]. It was found [131, 137] that ssDNA is more flexible and can reach a larger extension per base pair than dsDNA. Therefore, the Young's modulus of the dsDNA is greater than that of the ssDNA and the single-fixed dsDNA in which the end of one strand was left free [137]. It is seen (Table 3) that the values of Young's modulus obtained from the measurements on small fragments of DNA are significantly smaller than that determined from stretching experiments on long DNA. Additionally, experiments showed [107, 140] that the Young's modulus of dsRNA is approximately two times lower compared to that of dsDNA. The Poisson's ratio has been accepted for DNA and RNA to be in the range of 0.33–0.4 [141].

Table 2

Geometrical and elastic properties of viruses

Virus	Inner radius (nm)	Thickness (nm)	Geometry	Genome	Young's modulus (GPa)	Year	Reference	Comments
TMV	2	7	Cylinder	ssRNA	1.1	1997	[41]	Axial
TMV	2	7	Cylinder	ssRNA	6.8	2007	[77]	Axial
TMV	2	7	Cylinder	ssRNA	1.0	2008	[78]	Radial
TMV	2	7	Cylinder	ssRNA	1.3	2020	[79]	Radial
ϕ29	23.2	1.6	Sphere	dsDNA	1.8	2004	[62]	Prohead
ϕ29	23.2	1.6	Sphere	dsDNA	4.5	2007	[17]	Prohead
CCMV	10.5	3.8	Sphere	ssRNA	0.14	2006	[63]	Empty WT
CCMV	10.5	3.8	Sphere	ssRNA	0.19	2006	[63]	Empty SubE
CCMV	10.4	2.8	Sphere	ssRNA	0.28	2007	[17]	Empty WT
CCMV	10.4	2.8	Sphere	ssRNA	0.36	2007	[17]	Empty SubE
CCMV	10.5	3.5	Sphere	ssRNA	0.22	2008	[72]	Native
STMV	8.5	3	Sphere	ssRNA	3.3	2007	[68]	Wet crystal
STMV	8.5	3	Sphere	ssRNA	10.0	2007	[68]	Dry crystal
MLV	46	4	Sphere	ssRNA	1.0	2006	[66]	Mature
MLV	30	20	Sphere	ssRNA	0.23	2006	[66]	Immature
HIV-1	45	5	Sphere	ssRNA	0.44	2007	[120]	Mature
HIV-1	25	25	Sphere	ssRNA	0.93	2007	[120]	Immature
λ	29.5	1.8	Sphere	dsDNA	1.0	2007	[64]	
HSV-1	49.5	4	Sphere	dsDNA	1.0	2009	[117]	

Continued of table 2

MVM	11.5	2	Sphere	ssDNA	1.25	2006	[67]	
HBV	11.9	2.4	Sphere	dsDNA	0.37	2008	[70]	
HBV	12	2.5	Sphere	dsDNA	0.26	2010	[81]	
WIV	66	4	Sphere	dsDNA	7.0	2008	[69]	
HK97	28.2	1.8	Sphere	dsDNA	1.0	2012	[65]	
NV	14.5	9	Sphere	ssRNA	0.03	2010	[118]	pH 4.0
NV	10.85	2.7	Sphere	ssRNA	0.2	2011	[119]	
Influenza	47.5	5	Sphere	ssRNA	0.045	2011	[75]	
Influenza	46.9	3.1	Sphere	ssRNA	0.03	2012	[121]	
P2	26	4	Sphere	dsDNA	1.17	2021	[122]	Fully filled
P2	26	4	Sphere	dsDNA	0.87	2021	[122]	2/3 filled
SARS-CoV-2	42.5	5	Sphere	ssRNA	0.2	2020	[123]	Without spike
SARS-CoV-2	48	4	Sphere	ssRNA	0.03 or 0.06	2021	[124]	Without spike

Table 3

Elasticity of nucleic acid polymers

Genome	Young's modulus (MPa)	Test	Technics	Year	Reference	Comments
dsDNA	346	Stretching	Optical	1996	[130]	λ DNA
dsDNA	300	Stretching	Optical	2002	[131]	λ DNA
ssDNA	240	Stretching	Optical	2002	[131]	λ DNA
dsDNA	207	Nanoindentation	AFM	2004	[132]	λ DNA
dsDNA	393	Twisting-stretching	Magnetic	2006	[133]	
dsDNA	260	Nanoindentation	AFM	2007	[134]	λ DNA
dsDNA	300	Stretching	Optical	2009	[135]	λ DNA
dsDNA	138	Nanoindentation	AFM	2019	[136]	
ssDNA	18	Nanoindentation	AFM	2010	[137]	Small DNA
dsDNA	45	Nanoindentation	AFM	2010	[137]	Small single-fixed DNA
dsDNA	55	Nanoindentation	AFM	2010	[137]	Small double-fixed DNA
ssDNA	75	Nanoindentation	AFM	2014	[138]	DNA origami
dsRNA	200	Stretching	Optical	2011	[139]	
dsRNA	159	Stretching	Optical	2013	[140]	150 mM NaCl
dsDNA	298	Stretching	Optical	2013	[140]	150 mM NaCl
dsRNA	201	Stretching	Optical	2013	[140]	300 mM NaCl
dsDNA	371	Stretching	Optical	2013	[140]	300 mM NaCl
dsRNA	217	Stretching	Optical	2013	[140]	500 mM NaCl
dsDNA	383	Stretching	Optical	2013	[140]	500 mM NaCl

The structural and atomistic defects may occur in the virus as the indicators of damage influenced by environment. Development of damage causes the reduction of virus stiffness. In this regard, the Young's modulus of virus at the current instant of time can be presented as

$$E = E_0(1-\omega) \tag{4}$$

Here ω is the Kachanov-Rabotnov damage parameter [27, 60, 61, 142] which is increasing with time from the initial value $\omega = \omega_0$ at the reference instant to the final value $\omega = \omega_*$ at the instant of rupture (or destructuration) of viruses, E_0 is the Young's modulus of virus at the reference instant of time. In the simplest case it is possible to accept that $\omega_0 = 0$ and $\omega_* = 1$. Also, healing of damage affected by the environmental factors may occur during the virus life. Therefore, in general, the Young's modulus of virus at the current instant of time can be written as follows

$$E = E_0\left[1 - \omega(1-h)\right] \qquad (5)$$

Here h is the healing parameter [143, 144, 145, 146] which is increasing with time from the initial value $h = h_0$ at the reference instant to the final value $h = h_*$. In the simplest case we can accept that $h_0 = 0$ and $h_* = 1$.

The Young's modulus defines the resistance of virus to elastic deformation. However, it is not enough to reproduce the nonlinear mechanical behavior of viruses. So, Fig. 12 shows the force-indentation curves of empty prohead of the $\phi 29$ virus adsorbed on a modified glass surface [74]. The AFM nanoindetation tests were carried out with the initial prestress on upright and laid down proheads of $\phi 29$. Figure 13 demonstrates the nanoindentation studies under loading and unloading for empty capsid of CCMV with SubE protein mutant on a glass substrate [63]. The results of the AFM nanoindentation measurements [63] at increasing loading rates in the range of 6–6000 nm/s are given in Fig. 14 for empty CCMV (a) and HK97 (b) capsids.

Now, a number of comments need to be made in reference to Figs. 12–14. First, the nanoindentation results with the initial prestress given for one and the same location indicate that the $\phi 29$ virus is stiffer in compression than in tension. In other words, $\phi 29$ is excellent in resisting compression. One source of tension elements in virus is related to the natural ability of the protein-genome complexes to generate an opposing tension force that will return to its upstretched state [147]. The next source of tension elements is the chromatin-genome association that is highly extensible in the attempt to return to a state of maximal entropy [147]. Thus, viruses belong to a broad class of natural and artificial materials with different behavior under tension, and compression [1, 2, 3, 27, 61, 148, 149, 150, 151, 152, 153, 154, 155, 156, 157, 158, 159, 160]. Second, the $\phi 29$ shells are approximately two times stiffer along the short axis (particle lying on its side) than along the long one (upright particle). Obviously that stiffness of pentamers is different from that of hexamers. Also, the force-indentation curves exhibit large differences when the MVM capsids are compressed along the two-, three-, and fivefold symmetry axes [67, 161]. Thus, it is necessary to take into account the initial spherical anisotropy, and, in general, spherical virus may be a triclinic, monoclinic, orthotropic, tetragonal, transversely isotropic or cubic material [162]. Third, the experimental data under unloading show clearly that the total strain for viruses includes the permanent plastic part. Fourth, the force-indentation curves at the increasing loading rates give the possibility to reproduce the creep behavior of viruses. Hence, creep has been considered as a time dependent irreversible deformation process. Finally, fracture of viruses observed in experiments is related to the bond breaking. There are two types of fracture in viruses [128]. Brittle fracture observed in TMV, MVM and HSV-1 [128] occurs at the failure strain of about 0.05 [163]. Ductile fracture of SARS-CoV-2, CCMV and HBV [124, 128] corresponds to the failure strain of about 1.7 [124]. The failure mode of NV, $\phi 29$, λ and HK97 [128] undergoes a transition from brittle fracture to ductile flow. Thus, deformation of viruses influenced by environment has been accompanied by small or large strains.

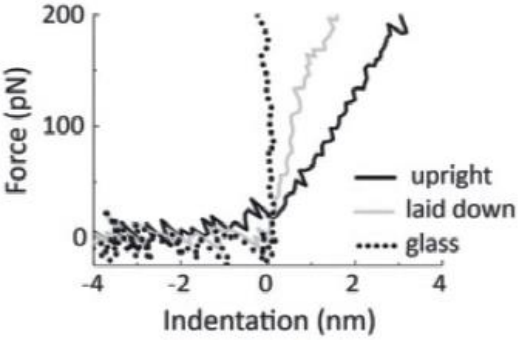

Fig. 12. The AFM nanoindentation experiments with the initial prestress for bacteriophage $\phi 29$ on different locations: glass substrate (dotted), upright configuration (grey) and laid down configuration (black) [74]

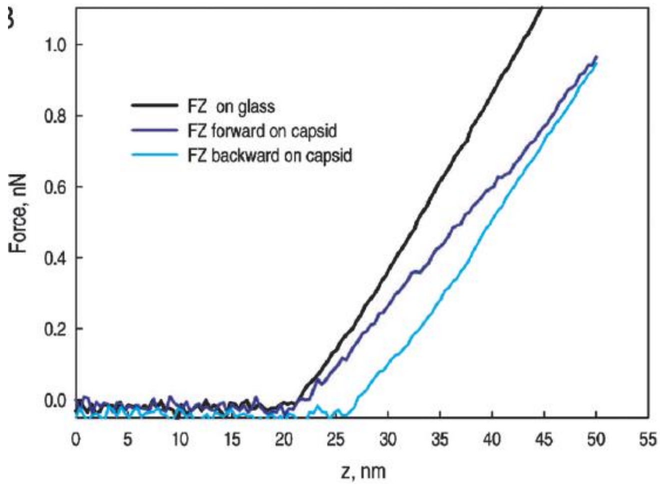

Fig. 13. The indenting force‒piezoactuator displacement curves of empty mutant CCMV capsid [63]

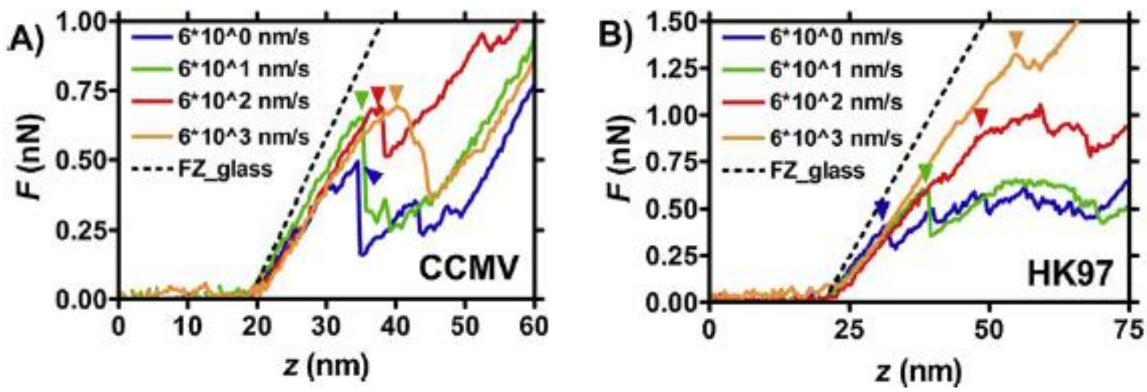

Fig. 14. The indenting force‒actuator displacement curves at increasing loading rates: CCMV (a) and HK97 (b) [63]

Also, swelling occurs in viruses when there are changes in the pH of the solution, release of bound ions (such as, Ca^{2+}) or different modifications of charge on the viral shells [164]. Such phenomenon was observed experimentally, and the radial expansion was found to be 8 % (STMV) [165], 10 % (CCMV) [166], 12 % (BMV) [167, 168] and 14 % (tomato bushy stunt virus) [169]. Electrostatic interaction among the negatively charged ssRNA/DNA molecule and the positively charged domains of the capsid proteins can be accepted as the basic physical mechanism of swelling in viruses [170, 171]. Environmentally induced shrinkage can also occur in viruses [172, 173, 174, 175]. Both swelling and shrinkage can be described taking into account the piezoelectric response of viruses [176, 177].

In general, the mechanical properties discussed above give the information which is necessary to find the relationship between the viral structure, environmental effect and biological function of viruses.

Constitutive modeling and simulation. Let us consider virus as the isotropic material with different behavior in tension and compression. Then the initial (reference) configuration with coordinates $x_i\ (i=1,2,3)$ and the deformed (present) configuration with coordinates X_i will be used to identify the material point of virus at a given instant of time $t\ (t \neq 0)$ within the framework of solid mechanics at finite strains. Let $u_i(x_1, x_2, x_3, t)$ are the components of the displacement vector of the material point at time t in directions x_1, x_2, x_3, respectively; $u_i = X_i - x_i$; $i=1,2,3$.

The Cauchy-Green strain tensor can be defined as [178]:

$$\varepsilon_{ij} = 0.5\left(u_{i,j} + u_{j,i} + u_{k,i}u_{k,j}\right), \qquad (6)$$

and it is easy to obtain the material time derivative of this tensor, such as

$$\dot{\varepsilon}_{ij} = 0.5\left(\dot{u}_{i,j} + \dot{u}_{j,i} + u_{k,i}\dot{u}_{k,j} + u_{k,j}\dot{u}_{k,i}\right), \left(i,j,k = 1,2,3\right) \qquad (7)$$

Here the dot above the symbol denotes a material time derivative. The rate of strain tensor in the present configuration of virus can be written as follows [178]

$$d_{ij} = 0.5\left(\frac{\partial \dot{u}_i}{\partial X_j} + \frac{\partial \dot{u}_j}{\partial X_i}\right) \qquad (8)$$

Tensors $\dot{\varepsilon}_{ij}$ and d_{ij} are connected by the relations [178]:

$$\dot{\varepsilon}_{ij} = \frac{\partial X_k}{\partial x_i}\frac{\partial X_l}{\partial x_j} d_{kl} \qquad (9)$$

and

$$d_{ij} = \frac{\partial x_k}{\partial X_i}\frac{\partial x_l}{\partial X_j}\dot{\varepsilon}_{kl}\,. \qquad (10)$$

Let us assume the additive decomposition of the time derivative of the total Cauchy-Green strain tensor, as well as, of the rate of strain tensor in the present configuration of virus to a linear elastic part, nonlinear elastic part, plastic part, creep part and piezoelectric part, respectively, in the following form:

$$\dot{\varepsilon}_{ij} = \dot{\varepsilon}^{e}_{ij} + \dot{\varepsilon}^{ne}_{ij} + \dot{\varepsilon}^{p}_{ij} + \dot{\varepsilon}^{c}_{ij} + \dot{\varepsilon}^{pe}_{ij} \qquad (11)$$

and

$$d_{ij} = d^{e}_{ij} + d^{ne}_{ij} + d^{p}_{ij} + d^{c}_{ij} + d^{pe}_{ij}\,. \qquad (12)$$

A connection between the second Piola-Kirchhoff stress tensor τ_{ij} and the Cauchy stress tensor σ_{ij} in virus can be presented as [178]

$$\tau_{ij} = J\sigma_{kl}\frac{\partial x_i}{\partial X_k}\frac{\partial x_j}{\partial X_l} \qquad (13)$$

and

$$\sigma_{ij} = J^{-1}\tau_{kl}\frac{\partial X_i}{\partial x_k}\frac{\partial X_j}{\partial x_l}\,. \qquad (14)$$

Here J is the Jacobian of deformation, $J = \det \mathbf{F}$; $\mathbf{F}$ is the matrix of the deformation gradients in the present configuration at time t, $\mathbf{F} = \left[\frac{\partial X_i}{\partial x_j}\right] = \left[\delta_{ij} + u_{i,j}\right], \left(i,j = 1,2,3\right)$; δ_{ij} is the Kronecker delta.

In order to describe the mechanical behavior of virus, it is necessary to formulate the constitutive equations in the rate form. Unfortunately, the material time derivative of the Cauchy stress tensor, i.e. $\dot{\sigma}_{kl}$, is not objective stress rate, because it is affected by rigid-body motions. Therefore, the Truesdell derivative $\sigma^{\mathrm{Tr}}_{kl}$ of the Cauchy stress tensor σ_{kl} will be used below, because it is an objective measure. As known [178], the material derivative of the second Piola-Kirchhoff stress tensor and the Truesdell derivative of the Cauchy stress tensor are connected by the relation

$$\dot{\tau}_{ij} = J\sigma^{\mathrm{Tr}}_{kl}\frac{\partial x_i}{\partial X_k}\frac{\partial x_j}{\partial X_l} \qquad (15)$$

with similar structure to (13). Then the relation between $\sigma^{\mathrm{Tr}}_{kl}$ and d^{e}_{ij} can be accepted as follows

$$\sigma^{\mathrm{Tr}}_{kl} = A^{*}_{klrs}\left(d_{rs} - d^{ne}_{rs} - d^{p}_{rs} - d^{c}_{rs} - d^{pe}_{rs}\right). \qquad (16)$$

Here A^{*}_{klrs} is the fourth-rank tensor of the elastic constants. By substituting (16) into (15) and using (10) we have

$$\dot{\tau}_{ij} = A_{ijkl}\left(\dot{\varepsilon}_{kl} - \dot{\varepsilon}^{ne}_{kl} - \dot{\varepsilon}^{p}_{kl} - \dot{\varepsilon}^{c}_{kl} - \dot{\varepsilon}^{pe}_{kl}\right), \qquad (17)$$

where

$$A_{ijkl} = JA^{*}_{mnrs}\frac{\partial x_i}{\partial X_m}\frac{\partial x_j}{\partial X_n}\frac{\partial x_k}{\partial X_r}\frac{\partial x_l}{\partial X_s}\ \left(m,n,r,s = 1,2,3\right) \qquad (18)$$

It is easy to see that the condition of symmetry $A_{ijkl} = A_{klij}$ takes place. Alternative based on the Jaumann stress derivative [178] $\sigma^{\mathrm{J}}_{ij} = \dot{\sigma}_{ij} - \Omega_{ir}\sigma_{rj} + \sigma_{ir}\Omega_{rj}$ with the spin tensor $\Omega_{ij} = 0.5\left(\frac{\partial \dot{u}_i}{\partial X_j} - \frac{\partial \dot{u}_j}{\partial X_i}\right)$

instead of the Truesdell stress derivative in Eq. (16) does not provide the satisfaction of the symmetry condition $A_{ijkl} = A_{klij}$.

A constitutive relation between the kinematic tensor e_{kl} in the present configuration and the Kirchhoff stress tensor T_{kl} can be written in the following form [148, 149, 179]:

$$e_{ij} = e_0\left(\frac{aI_1\delta_{ij} + cT_{ij}}{T_2} + b\delta_{ij}\right). \qquad (19)$$

Here $T_{kl} = J\sigma_{kl}$; $e_0 T_e = T_{ii}e_{ii}$; $T_e = T_1 + T_2$; $T_1 = bI_1$; $T_2^2 = aI_1^2 + cI_2$; $I_1 = T_{ij}\delta_{ij}$; $I_2 = T_{ij}T_{ij}$; T_e is the Kirchhoff equivalent stress; e_0 is the scalar function which depends on T_e, as well as, on the Kachanov-Rabotnov damage parameter ω and the healing parameter *h*, and which identifies for each physical state of virus (nonlinear elasticity, plasticity, creep); T_1 and T_2^2 are the linear and quadratic invariants of the Kirchhoff stress; *a*, *b* and c are the material parameters.

Considering the particular case of the nonlinear elasticity of virus, the kinematic tensor $e_{kl} \equiv d_{kl}^{ne}$ can be introduced as the nonlinear elastic part of the rate of strain tensor in the present configuration, and, additionally, it is necessary to define e_0 as the function of T_e, ω and *h*, as well as, to specify the kinetic equations for ω and *h*. In the simplest case of the nonlinear deformation with damage growth, but, without healing of damage, it is possible to accept [154, 180] in Eq. (19) that

$$e_0 = \frac{T_e{}^n \omega^k}{(1-\omega)^m} \tag{20}$$

with some material parameters *n*, *k* and *m*.

For the plastic deformation of virus, it is necessary to assume that the kinematic tensor $e_{kl} \equiv d_{kl}^{p}$ is the plastic part of the rate of strain tensor in the present configuration, as well as, to define [148, 179] the condition of loading and, additionally, the conditions when $d_{kl}^{p}=0$ in the cases of elastic deformation, unloading or neutral loading.

In the case of the creep deformation of virus, the kinematic tensor $e_{kl} \equiv d_{kl}^{c}$ in Eq. (19) is the creep part of the rate of strain tensor in the present configuration, and the scalar function e_0 in Eq. (19) should be defined [149, 181] using T_e, ω and *h*.

The piezoelectric part of the rate of strain tensor in the present configuration can be written in the following form [182]

$$d_{ij}^{pe} = -S_{kij} \frac{\partial \dot{\phi}}{\partial X_k}, \tag{21}$$

where S_{kij} is the third-rank tensor of the piezoelectric constants, and ϕ is the electric potential in virus.

Now, a number of comments need to be made in reference to the constitutive model given by Eqs. 11, 12, 17, 19–21. First, the material parameters of the model can be found by means of the identification methods [183, 184] using the experimental data discussed above under tension, compression and shear. Second, the present model can be extended to the case of the anisotropic plasticity/creep hardening under repeated loading according to the approaches [185, 186, 187]. Third, the fatigue of viruses can be described through the evolution equations [188, 189, 190] of the fatigue damage. Finally, in the case of the initial anisotropy of viruses it is necessary to use the tensor relationship given in [191, 192, 193, 194] instead of Eq. (19). As marked recently [195], there is nothing more fundamental in nonlinear mechanics of anisotropic materials with tension-compression asymmetry than the constitutive framework [191–194] developed in the early 1980s. Furthermore, such constitutive framework was used in [196–207] for modeling of the natural and artificial materials, however, without referencing sources [191–194].

Analysis of stress distributions over time in viruses, damage/healing analysis and lifetime prediction studies of viruses are related to the consideration of the physically and geometrically nonlinear initial/ boundary value multiphysics problem [208]. A three-dimensional finite element model (Fig. 15) derived from the reconstruction of virus from CryoEM photos may help to effectively simulate the influences of environmental factors on the mechanical behavior of viruses. Then the constitutive framework given by Eqs. 11, 12, 17, 19–21 needs to be incorporated into ANSYS [90, 92, 96, 98], ABAQUS [208, 209] and in-house developed software [19, 21, 22, 28, 29, 210] in a form of the computer-based structural modeling tool. These software packages give the possibility to calculate the time-dependent multiaxial stress distribution, as well as, changes of damage parameter and healing parameter at a discrete site of virus under applied loading conditions (or piezoelectric impairments) as a function of virus parameters, environmental factors and virus infectivity, and additionally to predict the lifetime of virus. The identification of material parameters in a constitutive framework from the force-displacement data is related to a number of the methodological and numerical difficulties [211], and can be made using an optimization technique [183, 184] and finite element simulations. Note that the finite element studies show [17] that the highest stresses in the viral capsid can reach 760 MPa, although the tensile strength of typical proteins is 133 MPa [42]. Thus, the further research in this direction is necessary.

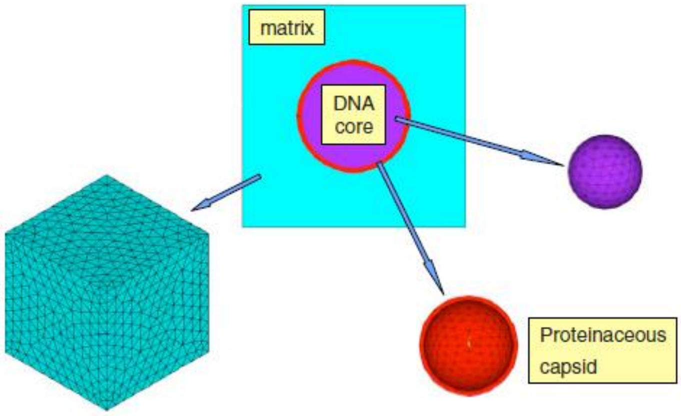

Fig. 15. A representative volume element of the host cell (matrix) embedded with the spherical virus with genome (DNA or RNA) [69]

In particular, the finite element analysis of the AFM nanoindentation data [212] for SARS-CoV-2 (Fig. 16 a) and SARS-CoV-1 (Fig. 16b) is critically important. It is seen (Fig. 16a, b) that the strength of SARS-CoV-2 is higher in comparison to SARS-CoV-1. Lifetime prediction studies of viruses might help to give a clear understanding of how neutralizing antibodies and T cells interact with the 2019 novel coronavirus SARS-CoV-2.

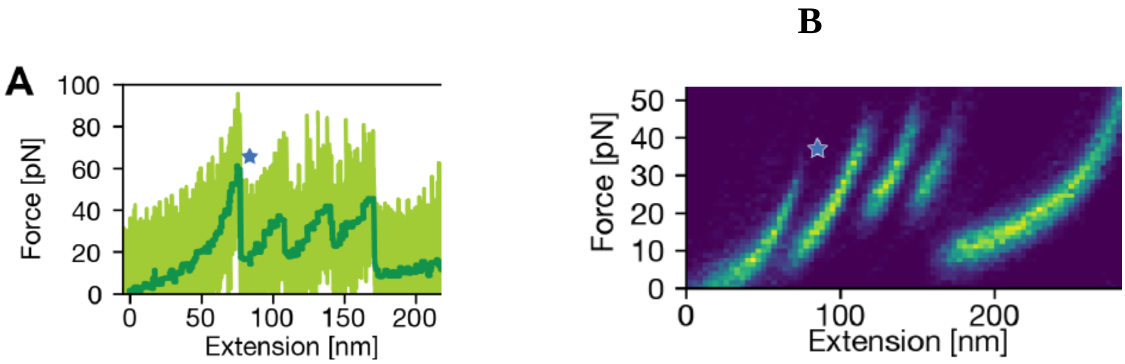

Fig. 16. The indenting force−piezoactuator displacement curves: SARS-CoV-2 (a) and SARS-CoV-1 (b) [212]

CONCLUSIONS

Knowledge of the mechanical response of viruses influenced by different environmental factors (mechanical loads, chemical changes, thermal changes, electromagnetic field and receptor binding on the host membrane) may assist medical specialists related to development of novel treatment strategies or development of vaccines for COVID 19.

An interdisciplinary structural modeling tool based on the nonlinear mechanics of viruses provides new insight into the lifetime of viruses and gives the possibility to develop the antiviral strategy.

REFERENCES

1. Martynenko OV, Zolochevsky OO, Allena R. Long term evolution of bone reconstruction with bone graft substitutes. The Journal of V. N. Karazin Kharkiv National University: Medicine. 2017; (33):107–18. https://periodicals.karazin.ua/medicine/article/view/9153.
2. Zolochevsky OO, Martynenko OV. Biomechanical analysis of tension-compression asymmetry, anisotropy and heterogeneity of bone reconstruction in response to periprosthetic fracture repair. The Journal of V. N. Karazin Kharkiv National University: Medicine. 2019; (37): 19–32. DOI: https://doi.org/10.26565/2313-6693-2019-37-03.

3. Zolochevsky A, Martynenko A. Neuromechanical characterization of brain damage in response to head impact and pathological changes. The Journal of V. N. Karazin Kharkiv National University: Medicine. 2020; (39): 5–25. DOI: https://doi.org/10.26565/2313-6693-2020-39-01.
4. Czekanski A, Martynenko AV, Zozulya VV. Modeling of heart muscles. In: Altenbach H, Öchsner A, editors. Encyclopedia of Continuum Mechanics. Berlin: Springer; 2020: 1713–23. DOI: https://doi.org/10.1007/978-3-662-55771-6.
5. Yuen KS, Ye ZW, Fung SY, Chan CP, Jin DY. SARS-CoV-2 and COVID-19: The most important research questions. Cell and Bioscience. 2020; 10: 40-1–5. DOI: https://doi.org/10.1186/s13578-020-00404-4.
6. Schrödinger E. What is Life? The Physical Aspect of the Living Cell. Cambridge: Cambridge University Press; 1944. 194 p.
7. Hinkle LE. The concept of «stress» in the biological and social sciences. The International Journal of Psychiatry in Medicine. 1974; 5 (4): 335–57. DOI: https://doi.org/10.2190/91DK-NKAD-1XP0-Y4RG.
8. Herrmann A, Sieben C. Single-virus force spectroscopy unravels molecular details of virus infection. Integrative Biology. 2015; 7 (6): 620–32. DOI: https://doi.org/10.1039/c5ib00041f.
9. Lee SY, Lim JS, Harris MT. Synthesis and application of virus-based hybrid nanomaterials. Biotechnology and Bioengineering. 2012; 109 (1): 16–30. DOI: https://doi.org/10.1002/bit.23328.
10. Rosenthal KS. Introduction to virology. In: Green L H, Goldman E, editors. Practical Handbook of Microbiology. 4th ed. Boca Raton: CRC Press; 2021. p. 704–21. DOI: https://doi.org/10.1201/9781003099277.
11. Kiss B, Mudra D, Török G, Mártonfalvi Z, Csík G, Herényi L, Kellermayer M. Single-particle virology. Biophysical Reviews. 2020; 12: 1141–54. DOI: https://doi.org/10.1007/s12551-020-00747-9.
12. Synowiec A, Szczepański A, Barreto-Duran E, Lie LK, Pyrc K. Severe acute respiratory syndrome coronavirus 2 (SARS-CoV-2): A systemic infection. Clinical Microbiology Reviews. 2021; 34 (2):e00133-20-1–32. DOI: https://doi.org/10.1128/CMR.00133-20.
13. Koontz D. The Eyes of Darkness. New York: Pocket Books; 1981. 128 p.
14. Roos WH. AFM nanoindentation of protein shells, expanding the approach beyond viruses. Seminars in Cell and Developmental Biology. 2018; 73: 145–52. DOI: https://doi.org/10.1016/j.semcdb.2017.07.044.
15. Carrillo PJP, Medrano M, Valbuena A, Rodriguez-Huete A, Castellanos M, Perez R, Mateu MG. Amino acid side chains buried along intersubunit interfaces in a viral capsid preserve low mechanical stiffness associated with virus infectivity. ACS Nano. 2017; 11 (2): 2194–208. DOI: https://doi.org/10.1021/acsnano.6b08549.
16. Roos WH, Bruinsma R, Wuite GJL. Physical virology. Nature Physics. 2010; 6 (10): 733–43. DOI: https://doi.org/10.1038/nphys1797.
17. Gibbons MM, Klug WS. Nonlinear finite-element analysis of nanoindentation of viral capsids. Physical Review E. 2007; 75 (3): 031901-1–11. DOI: https://doi.org/10.1103/PhysRevE.75.031901.
18. Zolochevsky AA. Allowance for differences in tension and compression for materials in the creep problems of shells. Dynamics and Strength of Machines. 1980; (32): 8–13.
19. Zolochevsky AA. Creep of thin shells for materials with different behavior in tension and compression [PhD thesis]. Kharkiv: Institute of Mechanical Engineering Problems of National Academy of Sciences of Ukraine; 1982. 198 p.
20. Zolochevskii AA. Method of calculating the strength of mine pipes formed from materials that behave differently under tension and compression. Strength of Materials. (1990); 22 (3): 422–8. DOI: https://doi.org/10.1007/BF00768204.
21. Altenbach H, Zolochevsky A. Kriechen dünner Schalen aus anisotropen Werkstoffen mit unterschiedlichem Zug-Druck-Verhalten. Forschung im Ingenieurwesen. 1991; 57 (6): 172–9. DOI: https://doi.org/10.1007/BF02575157.
22. Zolochevsky A, Sklepus S, Galishin A, Kühhorn A, Kober M. A comparison between the 3D and the Kirchhoff-Love solutions for cylinders under creep-damage conditions. Technische Mechanik. 2014; 34 (2): 104–13.
23. Naumenko K. On the use of the first order shear deformation models of beams, plates and shells in creep lifetime estimations. Technische Mechanik. 2000; 20 (3): 215–26.
24. Zolochevsky A, Galishin A, Kühhorn A, Springmann M. Transversal shear effect in moderately thick shells from materials with characteristics dependent on the kind of stress state under creep-damage conditions: Theoretical framework. Technische Mechanik. 2009; 29 (1): 38–47.
25. Galishin A, Zolochevsky A, Kühhorn A, Springmann M. Transversal shear effect in moderately thick shells from materials with characteristics dependent on the kind of stress state under creep-damage conditions: Numerical modeling. Technische Mechanik. 2009; 29 (1): 48–59.
26. Balandin AA, Fonoberov VA. Vibrational modes of nano-template viruses. Journal of Biomedical

Nanotechnology. 2005; 1 (1): 90–5. DOI: https://doi.org/10.1166/jbn.2005.005.
27. Zolochevsky AA, Sklepus AN, Sklepus SN. Nonlinear Solid Mechanics. Kharkiv: Garant; 2011. 719 p.
28. Zolochevsky A, Galishin A, Sklepus S, Parkhomenko L, Gnitko V, Kühhorn A, Leyens C. Benchmark creep tests for thermal barrier coatings. Journal of the National Technical University «Kharkiv Polytechnic Institute»: Machine-building and CAD. 2013; (23): 158–78.
29. Sklepus SN, Zolochevskii AA. A study of the creep damageability of tubular solid oxide fuel cell. Strength of Materials. 2014; 46 (1): 49–56. DOI: https://doi.org/10.1007/s11223-014-9514-1.
30. Wang J, Lapinski N, Zhang X, Jagota A. Adhesive contact between cylindrical (Ebola) and spherical (SARS-CoV-2) viral particles and a cell membrane. Mechanics of Soft Materials. 2020; 2: 11-1–9. DOI: https://doi.org/10.1007/s42558-020-00026-3.
31. Lidmar J, Mirny L, Nelson DR. Virus shapes and buckling transitions in spherical shells. Physical Review E. 2003; 68 (5): 051910-1–10. DOI: https://doi.org/10.1103/PhysRevE.68.051910.
32. Rodríguez RA, Pepper IL, Gerba CP. Application of PCR-based methods to assess the infectivity of enteric viruses in environmental samples. Applied and Environmental Microbiology. 2009; 75 (2): 297–307. DOI: https://doi.org/10.1128/AEM.01150-08.
33. Rodríguez-Lázaro D, Kovac K, Hernández M. Molecular detection of viruses in foods and food-processing environments. In: Cook N, editor. Viruses in Food and Water: Risks, Surveillance and Control. Cambridge: Woodhead Publishing; 2013. p. 49–78. DOI: https://doi.org/10.1533/9780857098870.2.49.
34. Zandi R, Dragnea B, Travesset A, Podgornik R. On virus growth and form. Physics Reports. 2020; 847: 1–102. DOI: https://doi.org/10.1016/j.physrep.2019.12.005.
35. Barrow E, Nicola AV, Liu J. Multiscale perspectives of virus entry via endocytosis. Virology Journal. 2013;10: 177-1–11. DOI: https://doi.org/10.1186/1743-422X-10-177.
36. Bao G, Bao XR. Shedding light on the dynamics of endocytosis and viral budding. Proceedings of the National Academy of Sciences. 2005; 102 (29): 9997–8. DOI: https://doi.org/10.1073/pnas.0504555102.
37. Gao H, Shi W, Freund LB. Mechanics of receptor-mediated endocytosis. Proceedings of the National Academy of Sciences. 2005; 102 (27): 9469–74. DOI: https://doi.org/10.1073/pnas.0503879102.
38. Smith DE, Tans SJ, Smith SB, Grimes S, Anderson DL, Bustamante C. The bacteriophage ϕ29 portal motor can package DNA against a large internal force. Nature. 2001; 413 (6857): 748–52. DOI: https://doi.org/10.1038/35099581.
39. Alsteens D, Newton R, Schubert R, Martinez-Martin D, Delguste M, Roska B, Müller D J. Nanomechanical mapping of first binding steps of a virus to animal cells. Nature Nanotechnology. 2017; 12 (2): 177–83. DOI: https://doi.org/101038/nnano.2016.228.
40. Jefferys EE, Sansom MS. Computational virology: Molecular simulations of virus dynamics and interactions. In: Greber U F, editor. Physical Virology. Vol. 1140. Advances in Experimental Medicine and Biology. Cham: Springer; 2019. p. 201–33. DOI: https://doi.org/10.1007/978-3-030-14741-9_10.
41. Falvo MR, Washburn S, Superfine R, Finch M, Brooks FP, Chi V, Taylor RM. Manipulation of individual viruses: Friction and mechanical properties. Biophysical Journal. 1997; 72 (3): 1396–403. DOI: https://doi.org/10.1016/ s0006-3495(97)78786-1.
42. Howard J. Mechanics of Motor Proteins and the Cytoskeleton. Sunderlan: Sinauer Associates; 2001. 373p.
43. Budday S, Ovaert TC, Holzapfel G A, Steinmann P, Kuhl E. Fifty shades of brain: A review on the mechanical testing and modeling of brain tissue. Archives of Computational Methods in Engineering. 2020; 27: 1187–230. DOI: https://doi.org/10.1007/s11831-019-09352-w.
44. Yengejeh SI, Kazemi SA, Öchsner A. Advances in mechanical analysis of structurally and atomically modified carbon nanotubes and degenerated nanostructures: A review. Composites Part B: Engineering. 2016; 86: 95–107. DOI: https://doi.org/10.1016/j.compositesb.2015.10.006.
45. Shokrieh MM, Rafiee R. Prediction of Young's modulus of graphene sheets and carbon nanotubes using nanoscale continuum mechanics approach. Materials & Design. 2010; 31 (2): 790–5. DOI: https://doi.org/10.1016/j.matdes. 2009.07.058.
46. Adhikari P, Li N, Shin M, Steinmetz NF, Twarock R, Podgornik R, Ching WY. Intra- and intermolecular atomic-scale interactions in the receptor binding domain of SARS-CoV-2 spike protein: Implication for ACE2 receptor binding. Physical Chemistry Chemical Physics. 2020; 22 (33): 18272–83. DOI: https://doi.org/10.1039/d0cp03145c.
47. Walls AC, Park YJ, Tortorici MA, Wall A, McGuire AT, Veesler D. Structure, function, and antigenicity of the SARS-CoV-2 spike glycoprotein. Cell. 2020; 181 (2): 281–92. DOI: https://doi.org/10.1016/j.cell.2020.02.058.
48. Gordon MS, Fedorov DG, Pruitt SR, Slipchenko LV. Fragmentation methods: A route to accurate calculations on large systems. Chemical Reviews. 2012; 112 (1): 632–72. DOI: https://doi.org/10.1021/cr200093j.

49. Zink M, Grubmüller H. Mechanical properties of the icosahedral shell of southern bean mosaic virus: A molecular dynamics study. Biophysical Journal. 2009; 96 (4): 1350–63. DOI: https://doi.org/10.1016/j.bpj.2008.11.028.
50. Zink M, Grubmüller H. Primary changes of the mechanical properties of southern bean mosaic virus upon calcium removal. Biophysical Journal. 2010; 98 (4): 687–95. DOI: https://doi.org/10.1016/j.bpj.2009.10.047.
51. May ER, Brooks CL. Determination of viral capsid elastic properties from equilibrium thermal fluctuations. Physical Review Letters. 2011; 106 (18): 188101-1–4. DOI: https://doi.org/10.1103/PhysRevLett.106.188101.
52. Larsson DS, Liljas L, van der Spoel D. Virus capsid dissolution studied by microsecond molecular dynamics simulations. PLoS Computational Biology. 2012; 8 (5): e1002502-1–8. DOI: https://doi.org/10.1371/journal.pcbi. 1002502.
53. Zhao G, Perilla JR, Yufenyuy EL, Meng X, Chen B, Ning J, Ahn J, Gronenborn AM, Schulten K, Aiken C, Zhang P. Mature HIV-1 capsid structure by cryo-electron microscopy and all-atom molecular dynamics. Nature. 2013; 497 (7451): 643–6. DOI: https://doi.org/10.1038/nature12162.
54. May ER. Recent developments in molecular simulation approaches to study spherical virus capsids. Molecular Simulation. 2014; 40 (10–11): 878–88. DOI: https://doi.org/10.1080/08927022.2014.907899.
55. Potoyan D, Papoian GA. The need for computational speed: State of the art in DNA coarse graining. In: Papoian G A, editor. Coarse-Grained Modeling of Biomolecules. Boca Raton: CRC Press; 2018. p. 271–96. DOI: https://doi.org/10.1201/9781315374284-7.
56. Arkhipov A, Freddolino PL, Schulten K. Stability and dynamics of virus capsids described by coarse-grained modeling. Structure. 2006; 14 (12): 1767–77. DOI: https://doi.org/10.1016/j.str.2006.10.003.
57. Cieplak M, Robbins MO. Nanoindentation of 35 virus capsids in a molecular model: Relating mechanical properties to structure. PloS One. 2013; 8 (6): e63640-1–15. DOI: https://doi.org/10.1371/journal.pone.0063640.
58. Kononova O, Snijder J, Brasch M, Cornelissen J, Dima RI, Marx KA, Wuite GJL, Roos WH, Barsegov V. Structural transitions and energy landscape for cowpea chlorotic mottle virus capsid mechanics from nanomanipulation in vitro and in silico. Biophysical Journal. 2013; 105 (8): 893–1903. DOI: https://doi.org/10.1016/j.bpj.2013. 08.032
59. Kononova O, Zhmurov A, Marx KA, Barsegov V. Mechanics of viruses. In: Papoian GA, editor. Coarse-Grained Modeling of Biomolecules. Boca Raton: CRC Press; 2018. p. 367–416. DOI: https://doi.org/10.1201/9781315374284-10.
60. Rabotnov YN. Solid Mechanics. 2nd ed. Moscow: Nauka; 1988. 712 p.
61. Altenbach H, Altenbach J, Zolochevsky A. Erweiterte Deformationsmodelle und Versagenskriterien der Werkstoffmechanik. Stuttgart: Deutsher Verlag für Grundstoffindustrie; 1995. 172 S.
62. Ivanovska IL, De Pablo PJ, Ibarra B, Sgalari G, MacKintosh FC, Carrascosa JL, Schmidt CF, Wuite GJL. Bacteriophage capsids: Tough nanoshells with complex elastic properties. Proceedings of the National Academy of Sciences. 2004; 101 (20): 7600–5. DOI: https://doi.org/10.1073/pnas.0308198101.
63. Michel JP, Ivanovska IL, Gibbons MM, Klug WS, Knobler CM, Wuite GJL, Schmidt CF. Nanoindentation studies of full and empty viral capsids and the effects of capsid protein mutations on elasticity and strength. Proceedings of the National Academy of Sciences. 2006; 103 (16): 6184–9. DOI: https://doi.org/10.1073/pnas.0601744103.
64. Ivanovska I, Wuite G, Jönsson B, Evilevitch A. Internal DNA pressure modifies stability of WT phage. Proceedings of the National Academy of Sciences. 2007; 104 (23): 9603–8. DOI: https://doi.org/10.1073/pnas.0703166104.
65. Snijder J, Ivanovska IL, Baclayon M, Roos WH, Wuite GJL. Probing the impact of loading rate on the mechanical properties of viral nanoparticles. Micron. 2012: 43 (12); 1343–50. DOI: https://doi.org/10.1016/j.micron. 2012. 04.011.
66. Kol N, Gladnikoff M, Barlam D, Shneck RZ, Rein A, Rousso I. Mechanical properties of murine leukemia virus particles: Effect of maturation. Biophysical Journal. 2006; 91 (2): 767–74. DOI: https://doi.org/10.1529/biophysj.105. 079657.
67. Carrasco C, Carreira A, Schaap IAT, Serena PA, Gomez-Herrero J, Mateu MG, De Pablo PJ. DNA-mediated anisotropic mechanical reinforcement of a virus. Proceedings of the National Academy of Sciences. 2006; 103 (37): 13706–11. DOI: https://doi.org/10.1073/pnas.0601881103.
68. Stephanidis B, Adichtchev S, Gouet P, McPherson A, Mermet A. Elastic properties of viruses. Biophysical Journal. 2007; 93 (4): 1354–9. DOI: https://doi.org/10.1529/biophysj.107.109033.
69. Hartschuh RD, Wargacki SP, Xiong H, Neiswinger J, Kisliuk A, Sihn S, Ward V, Vaia RA, Sokolov AP. How rigid are viruses. Physical Review E. 2008; 78 (2): 021907-1–9. DOI: https://doi.org/10.1103/PhysRevE.78.021907.

70. Uetrecht C, Versluis C, Watts NR, Roos WH, Wuite GJ, Wingfield PT, Steven AC, Heck AJR. High-resolution mass spectrometry of viral assemblies: Molecular composition and stability of dimorphic hepatitis B virus capsids. Proceedings of the National Academy of Sciences. 2008; 105 (27): 9216–20. DOI: https://doi.org/10.1073/pnas.0800406105
71. 71. Roos WH, Gertsman I, May ER, Brooks CL, Johnson JE, Wuite GJ. Mechanics of bacteriophage maturation. Proceedings of the National Academy of Sciences. 2012; 109 (7): 2342–7. DOI: https://doi.org/10.1073/pnas.1109590109
72. Gibbons MM, Klug WS. Influence of nonuniform geometry on nanoindentation of viral capsids. Biophysical Journal. 2008; 95 (8): 3640–9. DOI: https://doi.org/10.1529/biophysj.108.136176.
73. Klug WS, Roos WH, Wuite GJL. Unlocking internal prestress from protein nanoshells. Physical Review Letters. 2012; 109 (16): 168104-1–5. DOI: https://doi.org/10.1103/PhysRevLett.109.168104.
74. Carrasco C, Luque A, Hernando-Pérez M, Miranda R, Carrascosa JL, Serena PA, De Ridder M, Raman A, Gómez-Herrero J, Schaap IAT, Reguera D, De Pablo PJ. Built-in mechanical stress in viral shells. Biophysical Journal. 2011; 100 (4): 1100–8. DOI: https://doi.org/10.1016/j.bpj.2011.01.008.
75. Li S, Eghiaian F, Sieben C, Herrmann A, Schaap IA. Bending and puncturing the influenza lipid envelope. Biophysical Journal. 2011; 100 (3): 637–45. DOI: https://doi.org/10.1016/j.bpj.2010.12.3701.
76. Jiménez-Zaragoza M, Yubero MP, Martín-Forero E, Castón JR, Reguera D, Luque D, De Pablo PJ, Rodríguez J M. Biophysical properties of single rotavirus particles account for the functions of protein shells in a multilayered virus. Elife. 2018; 7:e37295-1–23. DOI: https://doi.org/10.7554/eLife.37295.
77. Schmatulla A, Maghelli N, Marti O. Micromechanical properties of tobacco mosaic viruses. Journal of Microscopy. 2007; 225 (3): 264–268. DOI: https://doi.org/10.1111/j.1365-2818.2007.01741.x.
78. Zhao Y, Ge Z, Fang J. Elastic modulus of viral nanotubes. Physical Review E. 2008; 78 (3): 031914-1–5. DOI: https://doi.org/10.1103/PhysRevE.78.031914.
79. Picotto GB, Vallino M, Ribotta L. Tip–sample characterization in the AFM study of a rod-shaped nanostructure. Measurement Science and Technology. 2020; 31 (8): 084001-1–19. DOI: https://doi.org/10.1088/1361-6501/ab7bc2.
80. Ankush A. Determination of prestress and elastic properties of virus capsids. Physical Review E. 2018; 97 (3): 032414-1–14. DOI: https://doi.org/10.1103/PhysRevE.97.032414.
81. Roos WH, Gibbons MM, Arkhipov A, Uetrecht C, Watts NR, Wingfield PT, Steven AC, Heck AJR, Schulten K, Klug WS, Wuite GJL. Squeezing protein shells: How continuum elastic models, molecular dynamics simulations, and experiments coalesce at the nanoscale. Biophysical Journal. 2010; 99 (4): 1175–81. DOI: https://doi.org/10.1016/j.bpj.2010.05.033.
82. Mkrtchyan S, Ing C, Chen JZ. Adhesion of cylindrical colloids to the surface of a membrane. Physical Review E. 2010; 81 (1): 011904-1–8. DOI: https://doi.org/0.1103/PhysRevE.81.011904.
83. Chen JZ, Mkrtchyan S. Adhesion between a rigid cylindrical particle and a soft fluid membrane tube. Physical Review E. 2010; 81 (4): 041906-1–9. DOI: https://doi.org/10.1103/PhysRevE.81.041906.
84. Cao SQ, Wei GH, Chen JZ. Bending energy of a vesicle to which a small spherical particle adhere: An analytical study. Chinese Physics B. 2015; 24 (9): 098702-1–9. DOI: https://doi.org/10.1088/1674-1056/24/9/098702.
85. Dragovich MA, Fortoul N, Jagota A, Zhang W, Schutt K, Xu Y, Sanabria M, Moyer DM, Moller-Tank S, Maury W, Zhang XF. Biomechanical characterization of TIM protein–mediated Ebola virus–host cell adhesion. Scientific Reports. 2019; 9: 267-1–13. DOI: https://doi.org/10.1038/s41598-018-36449-2.
86. Yuan H, Zhang S. Effects of particle size and ligand density on the kinetics of receptor-mediated endocytosis of nanoparticles. Applied Physics Letters. 2010; 96 (3): 033704-1–3. DOI: https://doi.org/10.1063/1.3293303.
87. Zhang S, Gao H, Bao G. Physical principles of nanoparticle cellular endocytosis. ACS Nano. 2015; 9 (9): 8655–71. DOI: https://doi.org/10.1021/acsnano.5b03184.
88. Gibbons MM, Chou T, D’orsogna MR. Diffusion-dependent mechanisms of receptor engagement and viral entry. The Journal of Physical Chemistry B. 2010; 114 (46): 15403–12. DOI: https://doi.org/10.1021/jp1080725.
89. Klinge S, Wiegold T, Aygün S, Gilbert RP, Holzapfel GA. On the mechanical modeling of cell components. PAMM. 2021; 20 (1): e202000129-1–4. DOI: https://doi.org/10.1002/pamm.202000129.
90. Zolochevsky A, Hop JG, Servant G, Foosnæs T, Øye H A. Creep and sodium expansion in a semigraphitic cathode carbon. In: Crepeau P N, editor. Light Metals. Warrendale: The Minerals, Metals and Materials Society; 2003. p. 595–602.
91. Zolochevsky A, Hop JG, Foosnæs T, Øye HA. Surface exchange of sodium, anisotropy of diffusion and diffusional creep in carbon cathode materials. In: Kvande H, editor. Light Metals. San Francisco: The Minerals, Metals and Materials Society; 2005. p. 745–750.

92. Eggen C, Lin YS, Goncharova G, Zolochevsky A. Diffusion characteristics of a supported lipid bilayer membrane on a dense cylindrical silica optical fibrous support. In: The 2009 AIChE Annual Meeting; 2009 Nov. 8–13; Nashville, USA. 2009. 20 p.
93. Zolochevsky A. Degradation of perovskite-type ceramic membranes determined by defect chemistry modeling and chemically induced stress analysis. Journal of the National Technical University «Kharkiv Polytechnic Institute»: Machine-building and CAD. 2008; (2): 95–104.
94. Zolochevsky A, Tkachuk NN, Viricelle JP, Pijolat C. Chemically induced stresses in the cathode of single chamber solid oxide fuel cell. Journal of the National Technical University «Kharkiv Polytechnic Institute»: Machine-building and CAD. 2007; 23: 148–57.
95. Zolochevsky AA, Goncharova GV, Minko AI, Shalashova IV. Modelling of diffusion induced stresses affected by the psychoactive media in the blood vessels of biomechanical system. Journal of the National Technical University «Kharkiv Polytechnic Institute»: Machine-building and CAD. 2008; (9): 90–7.
96. Zolochevsky A, Grabovskiy AV, Parkhomenko L., Lin YS. Coupling effects of oxygen surface exchange kinetics and membrane thickness on chemically induced stresses in perovskite-type membranes. Solid State Ionics. 2012; 212: 55–65. DOI: https://doi.org/10.1016/j.ssi.2012.02.003.
97. Zolochevsky A, Parkhomenko L, Kühhorn A. Analysis of oxygen exchange-limited transport and chemical stresses in perovskite-type hollow fibers. Materials Chemistry and Physics. 2012; 135 (2–3): 594–603. DOI: https://doi.org/10.1016/j.matchemphys.2012.05.031.
98. Zolochevsky A, Grabovskiy AV, Parkhomenko L, Lin YS. Transient analysis of oxygen non-stoichiometry and chemically induced stresses in perovskite-type ceramic membranes for oxygen separation. Journal of the National Technical University «Kharkiv Polytechnic Institute»: Machine-building and CAD. 2013; (1): 179–89.
99. Neuman KC, Nagy A. Single-molecule force spectroscopy: Optical tweezers, magnetic tweezers and atomic force microscopy. Nature Methods. 2008; 5 (6): 491–505. DOI: https://doi.org/10.1038/nmeth.1218.
100. Carrion-Vazquez M, Oberhauser AF, Fisher TE, Marszalek PE, Li H, Fernandez JM. Mechanical design of proteins studied by single-molecule force spectroscopy and protein engineering. Progress in Biophysics and Molecular Biology. 2000; 74 (1–2): 63–91. DOI: https://doi.org/10.1016/s0079-6107(00)00017-1.
101. Polishchuk VP, Budzanivska IG, Shevchenko TP, Andriychuk OM, Kompanets TA, Kondratyuk OA, Koroteeva GV, Molchanez OV, Harina AV, Shevchenko OV. Virology: A Tutorial for Laboratory Training. Kyiv: Comprint; 2017. 242 p.
102. Zhou G, Zhang B, Tang G, Yu XF, Galluzzi M. Cells nanomechanics by atomic force microscopy: Focus on interactions at nanoscale. Advances in Physics: X. 2021; 6 (1): 1866668-1–31. DOI: https://doi.org/10.1080/23746149.2020.1866668
103. De Pablo PJ, Schaap IAT. Atomic force microscopy of viruses. In: Greber U F, editor. Physical Virology. Vol. 1140, Advances in Experimental Medicine and Biology. Cham: Springer; 2019. p. 159–79. DOI: https://doi.org/10.1007/978-3-030-14741-9_8.
104. Hernando-Pérez M, Zeng C, Miguel M C, Dragnea B. Intermittency of deformation and the elastic limit of an icosahedral virus under compression. ACS Nano. 2019; 13 (7): 7842–9. DOI: https://doi.org/10.1021/acsnano.9b02133.
105. Faez S, Lahini Y, Weidlich S, Garmann RF, Wondraczek K, Zeisberger M, Schmidt MA, Orrit M, Manoharan VN. Fast, label-free tracking of single viruses and weakly scattering nanoparticles in a nanofluidic optical fiber. ACS Nano. 2015; 9(12): 12349–7. DOI: https://doi.org/10.1021/acsnano.5b05646.
106. Kondylis P, Schlicksup CJ, Zlotnick A, Jacobson SC. Analytical techniques to characterize the structure, properties, and assembly of virus capsids. Analytical Chemistry. 2018; 91 (1): 622–36. DOI: https://doi.org/10.1021/acs.analchem.8b04824.
107. Kriegel F, Ermann N, Lipfert J. Probing the mechanical properties, conformational changes, and interactions of nucleic acids with magnetic tweezers. Journal of Structural Biology. 2017; 197 (1); 26–36. DOI: https://doi.org/10.1016/j.jsb.2016.06.022.
108. Abels JA, Moreno-Herrero F, Van der Heijden T, Dekker C, Dekker NH. Single-molecule measurements of the persistence length of double-stranded RNA. Biophysical Journal. 2005; 88 (4): 2737–44. DOI: https://doi.org/10.1529/biophysj.104.052811.
109. Roos WH, Ivanovska IL, Evilevitch A, Wuite GJL. Viral capsids: Mechanical characteristics, genome packaging and delivery mechanisms. Cellular and Molecular Life Sciences. 2007; 64 (12): 1484–97. DOI: https://doi.org/10.1007/s00018-007-6451-1.
110. Hertz H. Über die Berührung fester elastischer Körper. Journal für die Reine und Angewandte Mathematik. 1881; 92: 156–71.

111. Rvachev VL, Protsenko VS. Contact Problems of the Theory of Elasticity for Non-Classical Regions. Kiev: Naukova Dumka; 1977. 235 p.
112. Borodich FM. The Hertz-type and adhesive contact problems for depth-sensing indentation. In: Bordas S P A, editor. Vol. 47. Advances in Applied Mechanics. London: Academic Press; 2014. p. 225–366, DOI: https://doi.org/10.1016/B978-0-12-800130-1.00003-5.
113. Sneddon IN. The relation between load and penetration in the axisymmetric Boussinesq problem for a punch of arbitrary profile. International Journal of Engineering Science. 1965; 3 (1): 47–57. DOI: https://doi.org/10.1016/0020-7225(65)90019-4.
114. Derjaguin BV, Muller VM, Toporov YP. Effect of contact deformations on the adhesion of particles. Journal of Colloid and Interface Science. 1975; 53 (2): 314–26. DOI: https://doi.org/10.1016/0021-9797(75)90018-1.
115. Johnson KL, Kendall K, Roberts A. Surface energy and the contact of elastic solids. Proceedings of the Royal Society of London A. 1971; 324 (1558): 301–13. DOI: https://doi.org/10.1098/rspa.1971.0141.
116. Dimitriadis EK, Horkay F, Maresca J, Kachar B, Chadwick RS. Determination of elastic moduli of thin layers of soft material using the atomic force microscope. Biophysical Journal. 2002; 82 (5): 2798–810. DOI: https://doi.org/10.1016/S0006-3495(02)75620-8.
117. Roos WH, Radtke K, Kniesmeijer E, Geertsema H, Sodeik B, Wuite GJ. Scaffold expulsion and genome packaging trigger stabilization of herpes simplex virus capsids. Proceedings of the National Academy of Sciences. 2009; 106 (24): 9673–8. DOI: https://doi.org/10.1073/pnas.0901514106.
118. Cuellar JL, Meinhoevel F, Hoehne M, Donath E. Size and mechanical stability of norovirus capsids depend on pH: A nanoindentation study. Journal of General Virology. 2010; 91 (10): 2449–56. DOI: https://doi.org/10.1099/vir.0.021212-0.
119. Baclayon M, Shoemaker GK, Uetrecht C, Crawford SE, Estes MK, Prasad BV, Heck AJR, Wuite GJL, Roos WH. Prestress strengthens the shell of Norwalk virus nanoparticles. Nano Letters. 2011; 11 (11): 4865–9. DOI: https://doi.org/10.1021/nl202699r.
120. Kol N, Shi Y, Tsvitov M, Barlam D, Shneck RZ, Kay MS, Rousso I. A stiffness switch in human immunodeficiency virus. Biophysical Journal. 2007; 92 (5): 1777–83. DOI: https://doi.org/10.1529/biophysj.106.093914.
121. Schaap IAT, Eghiaian F, des Georges A, Veigel C. Effect of envelope proteins on the mechanical properties of influenza virus. Journal of Biological Chemistry. 2012; 287 (49): 41078–88. DOI: https://doi.org/10.1074/jbc.m112.412726.
122. Choi SS, Kim KJ. Mechanical characterization of P2 bacteriophage by using Young's modulus measurements. AIP Advances. 2021; 11 (1): 015245-1–9. DOI: https://doi.org/10.1063/5.0035106.
123. Jasevičius R. Numerical modeling of coronavirus interaction mechanics with a host human cell. Mechanics of Advanced Materials and Structures. 2020 Dec; 1–28. DOI: https://doi.org/10.1080/15376494.2020.1853857.
124. Wierzbicki T, Li W, Liu Y, Zhu J. Effect of receptors on the resonant and transient harmonic vibrations of coronavirus. Journal of the Mechanics and Physics of Solids. 2021; 150: 104369-1–21. DOI: 10.1016/ j.jmps.2021.104369.
125. Reissner E. Stresses and small displacements of shallow spherical shells. II. Journal of Mathematics and Physics. 1946; 25 (1-4): 279–300. DOI: https://doi.org/10.1002/sapm1946251279.
126. Jia YF, Xuan FZ, Yang FQ. Numerical analysis of indentation of an elastic hemispherical shell. Journal of Mechanics. 2016; 32 (3): 245–53. DOI: https://doi.org/10.1017/jmech.2015.59.
127. Kasas S, Longo G, Dietler G. Mechanical properties of biological specimens explored by atomic force microscopy. Journal of Physics D: Applied Physics. 2013; 46 (13): 133001-1–12. DOI: https://doi.org/10.1088/0022-3727/46/13/133001.
128. Mateu MG. Mechanical properties of viruses analyzed by atomic force microscopy: A virological perspective. Virus Research. 2012; 168 (1–2): 1–22. DOI: https://doi.org/10.1016/j.virusres.2012.06.008.
129. Buzón P, Maity S, Roos WH. Physical virology: From virus self-assembly to particle mechanics. Wiley Interdisciplinary Reviews: Nanomedicine and Nanobiotechnology. 2020; 12 (4): e1613-1–22. DOI: https://doi.org/10.1002/ wnan.1613.
130. Smith SB, Cui Y, Bustamante C. Overstretching B-DNA: The elastic response of individual double-stranded and single-stranded DNA molecules. Science. 1996; 271 (5250): 795–9. DOI: https://doi.org/10.1126/science.271.5250.795.
131. Cocco S, Marko JF, Monasson R. Theoretical models for single-molecule DNA and RNA experiments: From elasticity to unzipping Comptes Rendus Physique. 2002; 3 (5): 569–84. DOI: https://doi.org/10.1016/S1631-0705(02)01345-2.
132. Morii T, Mizuno R, Haruta H, Okada T. An AFM study of the elasticity of DNA molecules. Thin Solid Films. 2004; 464: 456–8. DOI: https://doi.org/10.1016/j.tsf.2004.06.066.

133. Gore J, Bryant Z, Nöllmann M, Le MU, Cozzarelli NR, Bustamante C. DNA overwinds when stretched. Nature. 2006: 442 (7104), 836–9. DOI: https://doi.org/10.1038/nature04974.
134. Lin Y, Shen X, Wang J, Bao L, Zhang Z, Pang D. Measuring radial Young's modulus of DNA by tapping mode AFM. Chinese Science Bulletin. 2007: 52 (23); 3189–92. DOI: https://doi.org/10.1007/s11434-007-0475-7.
135. Pak YE, Kim DS, Marimuthu M, Kim S. Nanomechanics of biomolecules: Focus on DNA. Journal of Mechanical Science and Technology. 2009; 23 (7): 1949–58. DOI: https://doi.org/10.1007/s12206-009-0525-y.
136. Li L, Zhang X, Wang H, Lang Q, Chen H, Liu L Q. Measurement of radial elasticity and original height of DNA duplex using tapping-mode atomic force microscopy. Nanomaterials. 2019; 9 (4): 561-1–10. DOI: https://doi.org/10.3390/nano9040561.
137. Nguyen TH, Lee SM, Na K, Yang S, Kim J, Yoon ES. An improved measurement of dsDNA elasticity using AFM. Nanotechnology. 2010; 21 (7): 075101-1–7. DOI: https://doi.org/10.1088/0957-4484/21/7/075101.
138. Li L, Liu L, Tabata O, Li W J. Elasticity measurement of DNA origami nanotube in liquid with tapping mode AFM. In: The 9th IEEE International Conference on Nano/micro Engineered and Molecular Systems (NEMS). New York: IEEE; 2014. p. 684–7. DOI: https://doi.org/10.1109/nems.2014.7031669.
139. Brown ER, Mendoza EA, Kuznetsova Y, Neumann A, Brueck SRJ. High-resolution THz spectroscopy to measure strong THz absorption signatures of si-RNA in solution. In: Pereira M F, Shulika O, editors.Terahertz and Mid Infrared Radiation: Generation, Detection and Applications. Dordrecht: Springer; 2011. p. 15–22. DOI: https://doi.org/10.1007/978-94-007-0769-6_3.
140. Herrero-Galán E, Fuentes-Perez M E, Carrasco C, Valpuesta JM, Carrascosa JL, Moreno-Herrero F, Arias-Gonzalez J R. Mechanical identities of RNA and DNA double helices unveiled at the single-molecule level. Journal of the American Chemical Society. 2013; 135 (1): 122–31. DOI: https://doi.org/10.1021/ja3054755.
141. Liangruksa M, Laomettachit T, Wongwises S. Theoretical study of DNA's deformation and instability subjected to mechanical stress. International Journal of Mechanical Sciences. 2017; 130: 324–30. DOI: https://doi.org/10.1016/j.ijmecsci.2017.06.017.
142. Kachanov L. Introduction to Continuum Damage Mechanics. Dordrecht: Springer; 1986. 135p. DOI: https://doi.org/10.1007/978-94-017-1957-5.
143. Winter W, Heckmann SM, Weber HP. A time-dependent healing function for immediate loaded implants. Journal of Biomechanics. 2004; 37 (12): 1861–7. DOI: 10.1016/j.jbiomech.2004.02.033
144. Barbero E J, Greco F, Lonetti P. Continuum damage-healing mechanics with application to self-healing composites. International Journal of Damage Mechanics. 2005; 14 (1): 51–81. DOI: 10.1177/1056789505045928
145. Darabi M K, Al-Rub R K A, Little D N. A continuum damage mechanics framework for modeling micro-damage healing. International Journal of Solids and Structures. 2012; 49 (3–4):492–513. DOI: https://doi.org/10.1016/j.ijsolstr.2011.10.017.
146. Voyiadjis GZ, Oucif C, Kattan PI, Rabczuk T. Damage and healing mechanics in plane stress, plane strain, and isotropic elasticity. International Journal of Damage Mechanics. 2020; 29 (8): 1246–70. DOI: https://doi.org/10.1177/1056789520905347.
147. Bloom KS. Beyond the code: The mechanical properties of DNA as they relate to mitosis. Chromosoma. 2008; 117 (2): 103–10. DOI: https://doi.org/10.1007/s00412-007-0138-0.
148. Zolochevskii AA. Modification of the theory of plasticity of materials differently resistant to tension and compression for simple loading processes. Soviet Applied Mechanics. 1988; 24 (12): 1212–7. DOI: https://doi.org/10.1007/bf00887929
149. Zolochevskii AA. Effect of the type of loading on the creep of isotropic strain-hardening materials. Soviet Applied Mechanics. 1988; 24 (2): 185–91. DOI: https://doi.org/10.1007/bf00883831.
150. Zolochevskij AA. Kriechen von Konstruktionselementen aus Materialien mit von der Belastung abhängigen Charakteristiken. Technische Mechanik. 1988; 9 (3): 177–84.
151. Altenbach H, Zolochevsky AA. Eine energetische Variante der Theorie des Kriechens und der Langzeitfestigkeit für isotrope Werkstoffe mit komplizierten Eigenschaften. Zeitschrift für Angewandte Mathematik und Mechanik. 1994; 74 (3): 189–99. DOI: https://doi.org/10.1002/zamm.19940740311.
152. Mahnken R. Creep simulation of asymmetric effects by use of stress mode dependent weighting functions. International Journal of Solids and Structures. 2003; 40 (22): 6189–209. DOI: https://doi.org/10.1016/s0020-7683(03)00388-3.
153. Betten J, Sklepus A, Zolochevsky A. A constitutive theory for creep behavior of initially isotropic materials sustaining unilateral damage. Mechanics Research Communications. 2003; 30 (3): 251–6. DOI: https://doi.org/10.1016/s0093-6413(03)00002-8.

154. Zolochevsky A, Yeseleva E, Ehlers W. An anisotropic model of damage for brittle materials with different behavior in tension and compression. Forschung im Ingenieurwesen. 2005: 69 (3); 170–80. DOI: https://doi.org/10.1007/s10010-005-0150-6.
155. Huth A, Duddu R, Smith B. A generalized interpolation material point method for shallow ice shelves. 2: Anisotropic nonlocal damage mechanics and rift propagation. Journal of Advances in Modeling Earth Systems. 2021; 13: e2020MS002292-1–26. DOI: https://doi.org/10.1029/2020MS002292.
156. Jin S, Harmuth H. Asymmetric creep modeling of common refractory ceramics with high temperature wedge splitting test. Engineering Fracture Mechanics. 2021; 252: 107819-1–12. DOI: https://doi.org/10.1016/j.engfracmech.2021. 107819.
157. Ju X, Mahnken R, Xu Y, Liang L, Zhou W. A nonuniform transformation field analysis for composites with strength difference effects in elastoplasticity. International Journal of Solids and Structures. 2021; 228: 111103-1–16. DOI: https://doi.org/10.1016/j.ijsolstr.2021.111103.
158. Yang Y, Zhan L, Liu C, Xu Y, Li G, Wu X, Huang M, Hu Z. Tension-compression asymmetry of stress-relaxation ageing behavior of AA2219 alloy over a wide range of stress levels. Materials Science and Engineering A. 2021; 823: 141730-1–10. DOI: https://doi.org/10.1016/j.msea.2021.141730.
159. Zhang L, Lu M, Han L, Cao J. A model reduction method for nonlinear analysis of materials and structures with tension–compression asymmetric properties. Composite Structures. 2021; 262: 113613-1–13. DOI: https: //doi.org/10.1016/j. compstruct.2021.113613.
160. Zolochevskyi OO, Parkhomenko LO, Martynenko OV. Effect of non-stoichiometry and difference between the tensile and compressive moduli of elasticity of perovskite on the diffusion creep of a thick-walled perovskite cylinder. International Applied Mechanics. 2021; 57 (3): 336–46. DOI: https://doi.org/10.1007/s10778-021-01085-3.
161. Carrasco C, Castellanos M, de Pablo PJ, Mateu MG. Manipulation of the mechanical properties of a virus by protein engineering. Proceedings of the National Academy of Sciences. 2008; 105 (11): 4150–5. DOI: https://doi.org/10.1073_pnas.0708017105.
162. Ting TCT. The remarkable nature of radially symmetric deformation of spherically uniform linear anisotropic elastic solids. Journal of Elasticity. 1998: 53 (1); 47–64. DOI: https://doi.org/10.1023/A:1007516218827.
163. Buehler MJ, Yung YC. Deformation and failure of protein materials in physiologically extreme conditions and disease. Nature Materials. 2009; 8 (3): 175–88. DOI: https://doi.org/10.1038/nmat2387.
164. Božič AL, Šiber A. Electrostatics-driven inflation of elastic icosahedral shells as a model for swelling of viruses. Biophysical Journal. 2018; 115 (5): 822–9. DOI: https://doi.org/10.1016/j.bpj.2018.07.032.
165. Kuznetsov YG, Larson SB, Day J, Greenwood A, McPherson A. Structural transitions of satellite tobacco mosaic virus particles. Virology. 2001; 284 (2): 223–34. DOI: https://doi.org/10.1006/viro.2000.0914.
166. Speir JA, Munshi S, Wang G, Baker TS, Johnson JE. Structures of the native and swollen forms of cowpea chlorotic mottle virus determined by X-ray crystallography and cryo-electron microscopy. Structure. 1995; 3 (1): 63–78. DOI: https://doi.org/10.1016/S0969-2126(01)00135-6.
167. Incardona NL, Kaesberg P. A pH-induced structural change in bromegrass mosaic virus. Biophysical Journal. 1964; 4 (1): 11–21. DOI: https://doi.org/10.1016/S0006-3495(64)86766-7.
168. Bond KM, Lyktey NA, Tsvetkova IB, Dragnea B, Jarrold MF. Disassembly intermediates of the brome mosaic virus identified by charge detection mass spectrometry. The Journal of Physical Chemistry B. 2020; 124 (11): 2124–31. DOI: https://doi.org/10.1021/acs.jpcb.0c00008.
169. Witz J, Brown F. Structural dynamics, an intrinsic property of viral capsids. Archives of Virology. 2001; 146 (12): 2263–74. DOI: https://doi.org/10.1007/s007050170001.
170. Cherstvy AG. Electrostatic interactions in biological DNA-related systems. Physical Chemistry Chemical Physics. 2011; 13 (21): 9942–68. DOI: https://doi.org/10.1039/c0cp02796k.
171. Mahalik JP, Muthukumar M. Langevin dynamics simulation of polymer-assisted virus-like assembly. The Journal of Chemical Physics. 2012; 136 (13): 04B602-1–13. DOI: https://doi.org/10.1063/1.3698408.
172. Lu B, Stubbs G, Culver JN. Carboxylate interactions involved in the disassembly of tobacco mosaic tobamovirus. Virology. 1996; 225 (1): 11–20. DOI: https://doi.org/10.1006/viro.1996.0570.
173. Culver JN. Tobacco mosaic virus assembly and disassembly: Determinants in pathogenicity and resistance. Annual Review of Phytopathology. 2002; 40 (1): 287–308. DOI: https://doi.org/10.1146/annurev.phyto.40.120301.102400.
174. Sachse C, Chen JZ, Coureux PD, Stroupe ME, Fändrich M, Grigorieff N. High-resolution electron microscopy of helical specimens: A fresh look at tobacco mosaic virus. Journal of Molecular Biology. 2007; 371 (3): 812–35. DOI: https://doi.org/10.1016/j.jmb.2007.05.088.
175. De Pablo PJ. Atomic force microscopy of virus shells. Seminars in Cell and Developmental Biology. 2018; 73: 199–208. DOI: https://doi.org/10.1016/j.semcdb.2017.08.039.

176. Yu SM. Squeezed virus produces electricity. Nature Nanotechnology. 2012; 7 (6): 343–4. DOI: https://doi.org/10.1038/nnano.2012.85.
177. Garrido A, Pashley RM, Ninham BW. Low temperature MS2 (ATCC15597-B1) virus inactivation using a hot bubble column evaporator (HBCE). Colloids and Surfaces B: Biointerfaces. 2017; 151: 1–10. DOI: https://doi.org/10.1016/j.colsurfb.2016.11.026.
178. Washizu K. Variational Methods in Elasticity and Plasticity. 3rd ed. Oxford: Pergamon Press; 1982. 630.
179. Zolochevskii AA. Verification of the governing equations for the nonlinear deformation of materials with different strengths in tension and compression. Journal of Applied Mechanics and Technical Physics. 1986; 27 (6): 913–7. DOI: https://doi.org/10.1007/bf00918838.
180. Zolochevsky A. Identification of damage variable in ceramic matrix composite with different behaviour in tension and compression. In: Bradt R C, Hasselman D P H, Munz D, Sakai M, Shevchenko V Y, editors. Vol. 12, Fracture Mechanics of Ceramics. Boston: Springer; 1996. p. 413–28. DOI: https://doi.org/10.1007/978-1-4615-5853-8_30.
181. Zolochevsky A, Obataya Y. Tension-compression asymmetry of creep and unilateral creep damage in aluminum for isothermal and nonisothermal processes. JSME International Journal A: Solid Mechanics and Material Engineering. 2001; 44 (1): 100–8. DOI: https://doi.org/10.1299/jsmea.44.100.
182. Miehe C, Rosato D. A rate-dependent incremental variational formulation of ferroelectricity. International Journal of Engineering Science. 2011; 49 (6): 466–96. DOI: https://doi.org/10.1016/j.ijengsci.2010.11.003.
183. Chen H, Cai LX. An elastoplastic energy model for predicting the deformation behaviors of various structural components. Applied Mathematical Modelling, 68, 405–421. DOI: https://doi.org/10.1016/j.apm.2018.11.024.
184. Ma J, Chen G, Ji L, Qian L, Dong S. A general methodology to establish the contact force model for complex contacting surfaces. Mechanical Systems and Signal Processing. 2020; 140: 106678-1–21. DOI: https://doi.org/10.1016/j.ymssp.2020.106678.
185. Zolochevsky A, Sklepus S, Kozmin Y, Kozmin A, Zolochevsky D, Betten J. Constitutive equations of creep under changing multiaxial stresses for materials with different behavior in tension and compression. Forschung im Ingenieurwesen. 2004; 68 (4): 182–96. DOI: https://doi.org/10.1007/s10010-003-0123-6.
186. Zolochevsky A, Voyiadjis GZ. Theory of creep deformation with kinematic hardening for materials with different properties in tension and compression. International Journal of Plasticity. 2005; 21 (3): 435–62. DOI: https://doi.org/10.1016/j.ijplas.2003.12.007.
187. Song Z, Komvopoulos K. An elastic–plastic analysis of spherical indentation: Constitutive equations for single-indentation unloading and development of plasticity due to repeated indentation. Mechanics of Materials. 2014; 76: 93–101. DOI: https://doi.org/10.1016/j.mechmat.2014.05.005.
188. Zolochevsky A, Obataya Y, Betten J. Critical plane approach with two families of microcracks for modelling of unilateral fatigue damage. Forschung im Ingenieurwesen. 2000; 66 (2): 49–56. DOI: https://doi.org/10.1007/s100100000036.
189. Zolochevsky A, Itoh T, Obataya Y, Betten J. A continuum damage mechanics model with the strain-based approach to biaxial low cycle fatigue failure. Forschung im Ingenieurwesen. 2000; 66 (2): 67–73. DOI: https://doi.org/10.1007/s100100000040.
190. Zolochevsky A, Stepchenko A, Betten J. A microcrack description of multiaxial low cycle fatigue. Technische Mechanik. 2001; 21 (2): 109–20.
191. Zolochevskii A A. Allowance for differences in strain resistance in the creep of isotropic and anisotropic materials. Journal of Applied Mechanics and Technical Physics. 1982; 23 (4): 591–6. DOI: 10.1007/BF00916729
192. Zolochevskii AA. Tensor relationship in the theories of elasticity and plasticity of anisotropic composite materials with different tensile and compressive strength. Mechanics of Composite Materials. 1985; 21 (1): 41–6. DOI: https://doi.org/10.1007/BF00611805.
193. Zolochevskii AA. Determining equations and some problems of the variable-modulus theory of elasticity of anisotropic materials. Journal of Applied Mechanics and Technical Physics. 1985; 26 (4): 572–8. DOI: https://doi.org/10.1007/BF01101644.
194. Zolochevskii AA. Theory of cylindrical shells of anisotropic materials of different moduli. Soviet Applied Mechanics. 1986; 22 (3): 230–5. DOI: https://doi.org/10.1007/BF00887243.
195. Pahr DH, Reisinger AG. A review on recent advances in the constitutive modeling of bone tissue. Current Osteoporosis Reports. 2020; 18: 696–704. DOI: https://doi.org/10.1007/s11914-020-00631-1.
196. Pasynok MA. Development of anisotropic creep analysis methods taking into account damage of flat structural elements of machines [PhD thesis]. Kharkiv: National Technical University «Kharkiv Polytechnic Institute»; 2000.193 p.
197. Schwiedrzik JJ, Wolfram U, Zysset PK. A generalized anisotropic quadric yield criterion and its

application to bone tissue at multiple length scales. Biomechanics and Modeling in Mechanobiology. 2013; 12 (6): 1155–68. DOI: https://doi.org/10.1007/s10237-013-0472-5.
198. Levrero-Florencio F, Margetts L, Sales E, Xie S, Manda K, Pankaj P. Evaluating the macroscopic yield behaviour of trabecular bone using a nonlinear homogenisation approach. Journal of the Mechanical Behavior of Biomedical Materials. 2016; 61: 384–96. DOI: https://doi.org/10.1016/j.jmbbm.2016.04.008.
199. Panyasantisuk J, Pahr DH, Zysset PK. Effect of boundary conditions on yield properties of human femoral trabecular bone. Biomechanics and Modeling in Mechanobiology. 2016; 15 (5): 1043–53. DOI: https://doi.org/10.1007/s10237-015-0741-6.
200. Schwiedrzik J, Raghavan R, Rüggeberg M, Hansen S, Wehrs J, Adusumalli RB, Zimmermann T, Michler J. Identification of polymer matrix yield stress in the wood cell wall based on micropillar compression and micromechanical modelling. Philosophical Magazine. 2016; 96 (32–34): 3461–78. DOI: https://doi.org/10.1080/14786435. 2016.1235292.
201. Wang J, Xiao Y. Some improvements on Sun–Chen's one-parameter plasticity model for fibrous composites. Part I: Constitutive modelling for tension–compression asymmetry response. Journal of Composite Materials. 2017; 51 (3): 405–18. DOI: https://doi.org/10.1177/0021998316644853.
202. Levrero-Florencio F, Manda K, Margetts L, Pankaj P. Effect of including damage at the tissue level in the nonlinear homogenisation of trabecular bone. Biomechanics and Modeling in Mechanobiology. 2017: 16 (5): 1681–95. DOI: https://doi.org/10.1007/s10237-017-0913-7.
203. Levrero-Florencio F, Manda K, Margetts L, Pankaj P. Nonlinear homogenisation of trabecular bone: Effect of solid phase constitutive model. Proceedings of the Institution of Mechanical Engineers H: Journal of Engineering in Medicine. 2017; 231 (5): 405–14. DOI: https://doi.org/10.1177/0954411916676220.
204. Stipsitz M, Zysset PK, Pahr DH. Efficient materially nonlinear μFE solver for simulations of trabecular bone failure. Biomechanics and Modeling in Mechanobiology. 2019; 19 (5): 861–74. DOI: https://doi.org/10.1007/s10237-019-01254-x.
205. Wang J, Xiao Y, Inoue K, Kawai M, Xue Y. Modeling of nonlinear response in loading-unloading tests for fibrous composites under tension and compression. Composite Structures. 2019; 207: 894–908. DOI: https://doi.org/10.1016/j.compstruct.2018.09.054.
206. Speed A, Groetsch A, Schwiedrzik JJ, Wolfram U. Extrafibrillar matrix yield stress and failure envelopes for mineralised collagen fibril arrays. Journal of the Mechanical Behavior of Biomedical Materials. 2020; 105:103563-1–39. DOI: https://doi.org/10.1016/j.jmbbm.2019.103563.
207. Xie Y, Xiao Y, Lv J, Zhang Z, Zhou Y, Xue Y. Influence of creep on preload relaxation of bolted composite joints: Modeling and numerical simulation. Composite Structures. 2020; 245: 112332-1–15. DOI: https://doi.org/10.1016/j.compstruct.2020.112332.
208. Zolochevsky A, Martynenko A, Kühhorn A. Structural benchmark creep and creep damage testing for finite element analysis with material tension–compression asymmetry and symmetry. Computers and Structures. 2012; 100-101: 27–38. DOI: https://doi.org/10.1016/j.compstruc.2012.02.021.
209. Zolochevsky A, Becker AA. Introduction to ABAQUS. Kharkiv: Business Investor Group; 2011. 48 p.
210. Zolochevsky A, Sklepus S, Hyde TH, Becker AA, Peravali S. Numerical modeling of creep and creep damage in thin plates of arbitrary shape from materials with different behavior in tension and compression under plane stress conditions. International Journal for Numerical Methods in Engineering. 2009;80 (11): 1406–36. DOI: https://doi.org/10.1002/nme.2663.
211. Maksudov F, Kononova O, Llauró A, Ortega-Esteban A, Douglas T, Condezo GN, San Martín C, Marx KA, Wuite GJ, Roos WH, De Pablo PJ, Barsegov V. Fluctuating nonlinear spring theory: Strength, deformability, and toughness of biological nanoparticles from theoretical reconstruction of force-deformation spectra. Acta Biomaterialia. 2021; 122: 263–77. DOI: https://doi.org/10.1016/j.actbio.2020.12.043.
212. Bauer MS, Gruber S, Hausch A, Milles LF, Nicolaus T, Schendel LC, Navajas PL, Procko E, Lietha D, Bernardi RC, Gaub HE, Lipfert J. A tethered ligand assay to probe SARS-CoV-2: ACE2 interactions. bioRxiv. 2021:1-21. DOI: https://doi.org/10.1101/2021.08.08.455468.

КВАНТОВЕ, МОЛЕКУЛЯРНЕ І КОНТИНУАЛЬНЕ МОДЕЛЮВАННЯ В НЕЛІНІЙНІЙ МЕХАНІЦІ ВІРУСІВ

Золочевський О. О.[A,B, C,D,E,F]***, Пархоменко С. С.***[B,C, D,E,F]***, Мартиненко О. В.***[A,C,D E,F]

А – концепція та дизайн дослідження; В – збір даних; С – аналіз та інтерпретація даних; D – написання статті; Е – редагування статті; F – остаточне затвердження статті

Вступ. Віруси – це велика група патогенів, які, як було встановлено, заражають тварин, рослини, бактерії та навіть інші віруси. Новий коронавірус 2019 року SARS-CoV-2 залишається постійною загрозою для населення. Віруси – біологічні об'єкти з нанометричними розмірами, зазвичай від кількох десятків до кількох сотень нанометрів. Вони розглядаються як біомолекулярні структури, що складаються з генетичного матеріалу (РНК або ДНК), білкової оболонки (капсида) із захисною функцією, а іноді і додаткової оболонки поверх капсида

Мета. Мета даного огляду – допомогти спрогнозувати реакцію і навіть деструкцію вірусів з урахуванням впливу різних факторів навколишнього середовища, таких як механічні навантаження, температурні зміни, електромагнітне поле, хімічні зміни та зв’язування з рецептором мембрани клітини-господаря. Ці фактори навколишнього середовища значно впливають на вірус.

Матеріали та методи. Дослідження вірусів і вірусоподібних структур проаналізовано з використанням моделей і методів нелінійної механіки. У зв'язку з цим розглянуті квантові, молекулярні і континуальні описи в механіці вірусів. Застосування методів маніпулювання окремими молекулами, таких як атомно-силова мікроскопія, оптичний пінцет і магнітний пінцет, обговорюється для визначення механічних властивостей вірусів. Особливу увагу приділено континуальній механіці пошкоджень–загоєння пошкоджень вірусів, білків і вірусоподібних структур. Також представлено конститутивне моделювання вірусів при великих деформаціях. Враховувалися нелінійна пружність, пластична деформація, повзучість, викликане навколишнім середовищем набухання (або усадка) і п’єзоелектричний відгук вірусів. Обговорюється інтеграція конститутивної моделі в ABAQUS, ANSYS і програмне забезпечення власної розробки

Результати і висновки. Зв’язок між структурою вірусу, навколишнім середовищем, інфекційністю і механікою вірусу може бути корисний для прогнозування відгуку і деструктуризації вірусів з урахуванням впливу різних чинників навколишнього середовища. Обчислювальний аналіз з використанням такого зв'язку може бути корисний для чіткого розуміння того, як нейтралізуючі антитіла і Т-клітини взаємодіють з новим коронавірусів 2019 року SARS-CoV-2.

КЛЮЧОВІ СЛОВА: *вірус, механіка, атомно-силова мікроскопія, напруга, деформація, пошкодження, загоєння, моделювання, симуляція*

ИНФОРМАЦІЯ ПРО АВТОРІВ

Золочевський Олександр, д.техн.н., зав. лабораторії, НВО «Політех», вул. О. Яроша, 14, Харків, Україна, 61145, e-mail: zolochevsky55@ukr.net, ORCID ID: https://orcid.org/0000-0001-6632-4292

Пархоменко Софія, наук. співробітник, НВО «Політех», вул. О. Яроша, 14, Харків, Україна, 61145, e-mail: antiape41@gmail.com

Мартиненко Олександр, д.фіз-мат.н., професор кафедри гігієни та соціальної медицини Харківського національного університету імені В. Н. Каразіна, майдан Свободи, 6, Харків, Україна, 61022, e-mail: Alexander.v.martynenko@karazin.ua, ORCID ID: https://orcid.org/0000-0002-0609-2220

Для цитування:

Золочевський ОО, Пархоменко СС, Мартиненко ОВ. КВАНТОВЕ, МОЛЕКУЛЯРНЕ І КОНТИНУАЛЬНЕ МОДЕЛЮВАННЯ В НЕЛІНІЙНІЙ МЕХАНІЦІ ВІРУСІВ. Вісник Харківського національного університету імені В. Н. Каразіна. Серія «Медицина». 2022: 44; С. 5–34; **DOI: 10.26565/2313-6693-2022-44-01**

Conflicts of interest: *author has no conflict of interest to declare.*
Конфлікт інтересів: *відсутній.*

Отримано: 18.02.2022року
Прийнято до друку: 25.05.2022 року
Received: 02.18.2022
Accepted: 05.25.2022